



Review

# A Perspective on Li/S Battery Design: Modeling and Development Approaches

Chase McCreary <sup>1</sup>, Yuhui An <sup>2</sup>, Sun Ung Kim <sup>1,\*</sup> and Yoon Hwa <sup>3,\*</sup><sup>1</sup> School of Engineering and Computer Science, Washington State University, Vancouver, WA 98686, USA; chase.mccreary@wsu.edu<sup>2</sup> School for Engineering of Matter, Transport and Energy, Arizona State University, Tempe, AZ 85287, USA; yuhuian@asu.edu<sup>3</sup> School of Electrical, Computer and Energy Engineering, Arizona State University, Tempe, AZ 85287, USA

\* Correspondence: sunung.kim@wsu.edu (S.U.K.); Yoon.Hwa@asu.edu (Y.H.)

**Abstract:** Lithium/sulfur (Li/S) cells that offer an ultrahigh theoretical specific energy of 2600 Wh/kg are considered one of the most promising next-generation rechargeable battery systems for the electrification of transportation. However, the commercialization of Li/S cells remains challenging, despite the recent advancements in materials development for sulfur electrodes and electrolytes, due to several critical issues such as the insufficient obtainable specific energy and relatively poor cyclability. This review aims to introduce electrode manufacturing and modeling methodologies and the current issues to be overcome. The obtainable specific energy values of Li/S pouch cells are calculated with respect to various parameters (e.g., sulfur mass loading, sulfur content, sulfur utilization, electrolyte-volume-to-sulfur-weight ratio, and electrode porosity) to demonstrate the design requirements for achieving a high specific energy of >300 Wh/kg. Finally, the prospects for rational modeling and manufacturing strategies are discussed, to establish a new design standard for Li/S batteries.



**Citation:** McCreary, C.; An, Y.; Kim, S.U.; Hwa, Y. A Perspective on Li/S Battery Design: Modeling and Development Approaches. *Batteries* **2021**, *7*, 82. <https://doi.org/10.3390/batteries7040082>

Academic Editor: Catia Arbizzani

Received: 14 September 2021

Accepted: 29 November 2021

Published: 2 December 2021

**Publisher's Note:** MDPI stays neutral with regard to jurisdictional claims in published maps and institutional affiliations.



**Copyright:** © 2021 by the authors. Licensee MDPI, Basel, Switzerland. This article is an open access article distributed under the terms and conditions of the Creative Commons Attribution (CC BY) license (<https://creativecommons.org/licenses/by/4.0/>).

## 1. Introduction

Climate change has become a key consideration of governments around the globe [1] as the frequency and severity of natural disasters continue to increase [2]. Electrification of transportation is a significant component in reducing greenhouse gas (GHG) emissions because fossil-fuel-based transportation accounts for 26% of GHG emissions in the United States (US) and 23.2% of GHG emissions in the European Union [3]. Lithium-ion batteries (LiBs) have been developed significantly since their initial commercialization in 1991 [4]. Their continued development has expanded their applications from handheld electronics to electric vehicles (EVs), grid-scale energy storage, and much more [5,6]. However, Li-ion technology has matured to such a degree that it approaches its theoretical limitations for energy storage capability [7]. So far, despite researchers' continued efforts, the electrification of freight transportation, which makes up 9% of US GHG emissions [8], has remained beyond the scope of LiBs due to their insufficient specific energy and high energy price (USD/Wh) [9,10]. This has prompted research beyond LiB technology to develop alternative chemistries that can theoretically exceed the performance of LiBs [11]. Lithium/sulfur (Li/S) batteries are among the most promising next-generation electrochemical chemistries. To date, the development of Li/S battery technology has been primarily guided through experimentation [12], but more recently, researchers have begun to adopt rational design techniques [13] based on modeling and rapid iteration to accelerate the commercialization. The development of physics-based electrochemical models for Li/S batteries has accelerated in recent years [12]. Various models from the atomic scale to the battery cell scale

have been developed to elucidate phenomena occurring at all scales. These models will be discussed in more detail later in the paper.

Li/S batteries possess exceptional specific energy and a standard open-circuit potential of 2.15 V [14]. The theoretical maximum specific energy of a Li/S battery is  $2600 \text{ W h kg S}^{-1}$  [15], assuming the sulfur is fully utilized. However, complete utilization is not technically feasible due to the sluggish reaction kinetics and the insulating properties of elemental sulfur [16,17]. In addition, the weight of other cell components such as current collectors, separator, electrolyte, and cell housing materials should be considered when estimating the actual specific energy of Li/S batteries. Considering practical cell design parameters, a more realistic projection estimates the specific energy of Li/S batteries at between 400 and  $500 \text{ W h kg}^{-1}$  [12,18]. Though still early in the research phase of development, this technology currently exceeds the peak specific energy of Li-ion cells by about  $100 \text{ W h kg}^{-1}$  [12,19]. Li/S batteries also show improved safety during operation under abuse conditions compared to LiBs. Nail penetration tests demonstrated no explosive energy release when punctured due to a solid insulating coating that forms from lithium polysulfide (Li-PS), thereby preventing an internal short circuit via the penetrator [20]. Furthermore, because of the chemical stability of the active materials in the completely discharged state, the cells can be stored indefinitely without experiencing damage and without hazard risk [21].

Cost is another distinct advantage of Li/S batteries. After the electrolyte, the transition metal oxide positive electrode is the most expensive component of LiBs, exceeding USD 100 per kg. In the case of Li/S cells, the sulfur electrode is the cheapest component at a combined cost of USD 0.13 per kg of sulfur, USD 3 per kg of carbon, and USD 7 per kg of a binder [22]. The low cost of the positive electrode is mainly associated with the abundance of sulfur in nature and the high production volume of sulfur as a common byproduct of petrochemical production processes [23]. Furthermore, as sulfur loading and sulfur utilization improve over time, the price per kilowatt-hour will decline further because these parameters are directly associated with the stored energy of the cell. Researchers expect cell costs to be as low as USD 70–100 per kg [16,24].

However, Li/S batteries have critical and fundamental challenges that hinder cell performance. Elemental sulfur ( $\text{S}_8$ ) and lithium sulfide ( $\text{Li}_2\text{S}$ ) (a sulfur compound existing in the discharged cell condition) are electrically insulating, with an intrinsic conductivity of  $5 \times 10^{-30} \text{ S cm}^{-1}$  at  $25^\circ\text{C}$  [25]. This characteristic has several implications for the functionality of Li/S cells. Primarily, the low conductivity directly inhibits the electrochemical reaction and limits active material utilization [26]. Furthermore, the low conductivity results in sluggish reaction kinetics in the lower discharge plateau region. This is the cause of incomplete electrochemical utilization of sulfur, reducing the cell capacity [27]. Finally, the sluggish kinetics lead to significant internal resistance and, therefore, a large polarization which reduces cell efficiency and limits rate capability [28]. The very low conductivity of sulfur would render the cell unusable if not addressed; therefore, a significant amount of research has gone into sulfur electrode design for Li/S batteries.

In recent years, efforts have focused on highly porous nanostructured two-dimensional (2D) [29–32] and three-dimensional (3D) [33,34] conductive matrixes, which act as a host structure for  $\text{S}_8$  and  $\text{Li}_2\text{S}$ . The conductive host matrix allows for high areal loading of sulfur to increase its utilization while efficiently transferring electrons to counteract its low electrical conductivity. A mesoporous structure is often constructed with a pore size between 2 and 50 nm. The small pore size mechanically inhibits the diffusion of larger lithium polysulfide (Li-PS) ions while still allowing for efficient Li-ion transport between the electrodes [29–34]. However, Li/S batteries undergo a volume change of about 80% during cycling [35], and the repeated expansion and contraction can lead to debonding of sulfur from the conductive carbon matrix. The debonded material becomes electrically isolated, resulting in permanent loss of material and gradual capacity fade [34,36]. Therefore, researchers focus on designing sulfur electrodes that can accommodate the

expansion while including binding additives to improve and maintain electrical contact during cycling [37–42].

Another fundamental challenge associated with Li/S batteries is the Li-PS shuttle effect [43,44]. The phenomenon is caused by the significant solubility of higher-order Li-PS species  $\text{Li}_2\text{S}_x$  ( $4 < x \leq 8$ ) [44]. While charging, as the lower-order Li-PS species ( $\text{Li}_2\text{S}_x$ ,  $1 \leq x \leq 4$ ) undergo a series of electrochemical reactions to higher-order Li-PS, they become increasingly soluble, eventually dissolving into solution. The concentration of the higher-order species is greater at the sulfur electrode, so they diffuse along the concentration gradient to the lithium electrode. When they reach the lithium electrode, they undergo a direct parasitic conversion reaction with the lithium metal electrode to split back into lower-order Li-PS. As these lower-order Li-PS are produced, the local concentration rises, and the species diffuse back to the sulfur electrode, thus completing one cycle of the continuous Li-PS shuttle mechanism [43–46]. This shuttle effect causes significant self-discharge and is detrimental to the cycle life of Li/S batteries [14,21]. The parasitic reaction at the lithium electrode occasionally produces insoluble  $\text{Li}_2\text{S}$  deposits on the surface of the lithium metal electrode, resulting in a permanent loss of active material and, in consequence, an irreversible loss in capacity [44,45]. Furthermore, the undesired side reactions at the lithium electrode erode the protective solid electrolyte interphase (SEI). This exposes lithium metal directly to the electrolyte, causing an imbalance in the overpotential across the heterogeneous reaction surface. The local overpotential drives dendrite nucleation and growth as lithium ions precipitate out of solution during charging [47]. Over time, these dendrites can grow large enough to puncture the separator, resulting in an internal short circuit. Furthermore, the exposed lithium metal is highly reactive with the Li-PS and most electrolytes, resulting in corrosion of the lithium electrode itself [14,21]. The shuttle effect also causes significant self-discharge while resting in the fully charged state. The soluble high-order Li-PS species tend to dissolve into solution and diffuse to the lithium electrode along concentration gradients. If uninterrupted, this process will continue until equilibrium between the sulfur and the lithium electrode is achieved. This results in a reversible loss of active material, which causes a decline in the open-circuit voltage and capacity over time [21,48]. As a result, researchers have focused on constraining the Li-PS shuttle effect at the sulfur electrode [49] by developing selective separators [50,51], redox mediating additives [30,52], and multi-functional binders [39,40]. To date, several review articles have been published on the development of functional materials and cell components, and more detailed information can be found in those reviews [25,53–58].

This review mainly focuses on modeling and manufacturing methodologies and their future challenges and proposes a systematic design approach for manufacturing attractively practical Li/S batteries. Specifically, we categorize our discussion into two following Sections: Section 2. Modeling methodologies, from density functional theory to continuum modeling, and Section 3. Challenges in the design and manufacturing of Li/S cell components. The issues associated with these topics and their corresponding solutions are discussed. This review also introduces the under-represented problems that must be addressed in the commercialization of Li/S batteries.

## 2. Modeling Methodologies

### 2.1. Density Functional Theory

Density functional theory (DFT) is a first-principles modeling technique applied at the atomic scale [59]. As a first-principles model, DFT accounts for the fundamental forces and interactions in quantum chemistry, such as van der Waals forces, activation energies, and bond strengths. DFT models provide insights into atomic structures and properties. For the sake of computational efficiency, DFT models operate using exchange–correlation functionals to estimate the interatomic interactions by way of electron orbital density [59]. Researchers have also applied ab initio molecular dynamics (AIMD) within the frame-work of DFT to describe the time-dependent interatomic interactions between multiple species, thus allowing more dynamic and complex models to be developed [60]. DFT models have

largely been used to develop electrode and separator materials by providing insights into the PS reaction mechanisms [61–63], structure [64], and binding/adsorption energy [65–67].

### 2.1.1. Application

The Li-PS shuttle phenomenon poses a challenge in the development of high-cycle-life Li/S batteries. This phenomenon is caused by the high solubility of the intermediate Li-PS species in organic solvents and the insufficient binding and confining properties of the sulfur host structure [44,49]. Thus, several studies have applied AIMD within a DFT framework to model the time-dependent phenomena of various electrode structures, including carbon nanofibers [68], carbon nanotubes [65], carbon nanospheres [69], carbon monolayers [70], metal–organic frameworks (MOF) [71], and graphene [65,66]. The DFT models have also been adapted to observe the adsorption energy associated with additional atomic features such as single dopants (N, O, S, P, B, F, Cl, Mo) [65,66], co-dopants (N–S, N–P, N–O, N–B, B–O) [34,65], and functional groups (–OH, –COOH, –NH<sub>2</sub>) [67] within the electrode host structure. These dopants impact the binding energy and organization of the Li-PS within the electrode structure by altering the dipole–dipole interactions at the re-action surface (see Figure 1) [65,66].

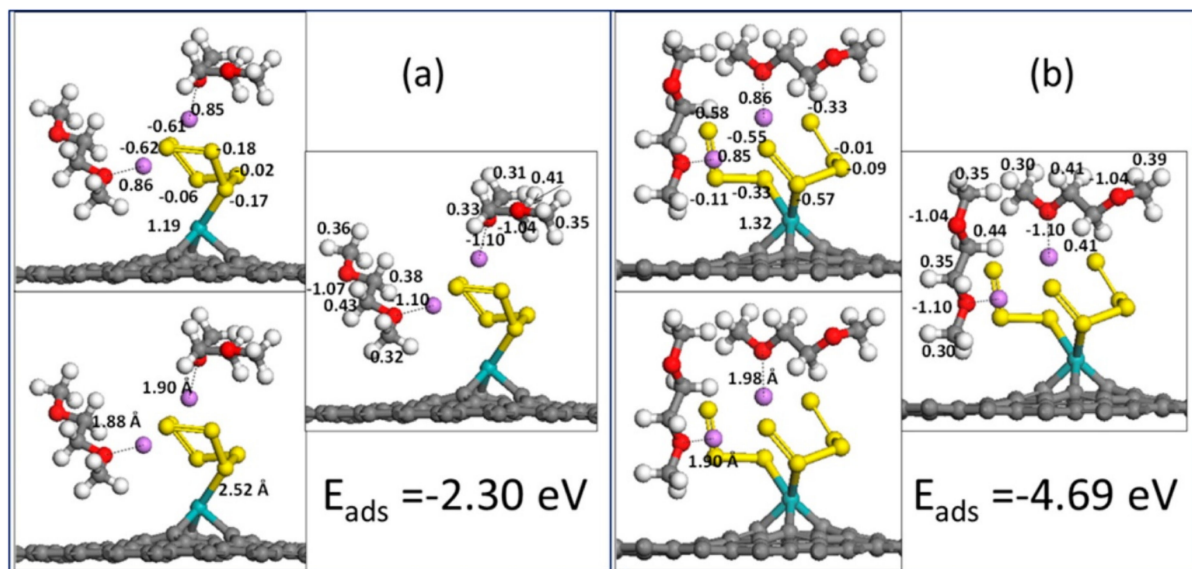


**Figure 1.** Adsorption energy of (a)  $\text{Li}_2\text{S}_6$  and (b)  $\text{Li}_2\text{S}_8$  in DME electrolyte on Mo-doped graphene substrate. Bader atomic charges are in units of e. Color code: Li-purple, S-yellow, Mo-blue, O-red, H-white, C-gray [66]. Reprinted with permission from Kamphaus, E.P.; Balbuena, P.B. Long-Chain Polysulfide Retention at the Cathode of Li-S Batteries. *J. Phys. Chem. C* 2016, 120, 4296–4305, doi:10.1021/acs.jpcc.5b12538. Copyright 2016 American Chemical Society.

DFT models have also been used to observe the binding energies of Li-PS on 2D monolayers ( $\text{BC}_2\text{N}$ ,  $\text{C}_2\text{N}$ ,  $\text{C}_3\text{N}$ ,  $\text{C}_3\text{B}$ , polymers) [70,72], transition metal carbides ( $\text{TiC}$ ,  $\text{WC}$ ), metal oxides ( $\text{TiO}_{2-x}$ ,  $\text{Fe}_2\text{O}_3$ ,  $\text{MnO}_2$ ,  $\text{Co}_3\text{O}_4$ ,  $\text{Al}_2\text{O}_3$ ,  $\text{CaO}$ ,  $\text{CeO}_2$ ,  $\text{La}_2\text{O}_3$ ,  $\text{MgO}$ ,  $\text{V}_2\text{O}_5$ ) [73,74], chlorides ( $\text{TiCl}_2$ ,  $\text{ZrCl}_2$ ), sulfides ( $\text{CoS}_3$ ,  $\text{TiS}_2$ ,  $\text{NiS}_2$ ,  $\text{VS}_2$ ,  $\text{ZrS}_2$ ,  $\text{NbS}_2$ ,  $\text{MoS}_2$ ) [72,74–76], and MOFs [71]. More recently, DFT models have characterized the binding and free energies of various electrocatalysts, including transition metal single-atom electrocatalysts (Fe, Mn, Ru, Zn, Co, Cu, V, Ag) [77], nanoparticles ( $\text{NiSe}_2$ ,  $\text{NiCo}_2$ ) [78], and nitrides ( $\text{VN}$ ,  $\text{TiN}$ ,  $\text{Fe}_2\text{N}$ ,  $\text{CoN}_4$ ) [68,69]. These catalysts lower the overpotential and  $\text{Li}_2\text{S}$  energy barrier, which in turn accelerates the reaction kinetics and improves sulfur utilization, rate capability, and cycle life [75]. DFT and AIMD simulations have also been used to elucidate the  $\text{Li}_2\text{S}/\text{Li}$  metal surface interactions, the nucleation and growth of a  $\text{Li}_2\text{S}$  film at the lithium surface [61], and the reaction phenomena occurring at the sulfur electrode [62]. Additionally, DFT and AIMD have been used to discover a layer-by-layer reaction pattern

during lithiation and delithiation [63] and to explain the impact of electrolyte chemistry on precipitation and electrocatalytic transformation of Li-PS in electrolytes [64].

### 2.1.2. Challenges

Several fundamental challenges associated with DFT simulations have thus far constrained the predictive capabilities of such models, thereby limiting their application in rational design. Instead, they have typically been guided by, or provided insights into, experimental findings [12]. Firstly, atomic-scale DFT models can only make predictions at the nanopore scale with current computational capabilities because of the computational cost. Generally, the DFT models could handle up to 100–200 atoms [59]. However, experimental findings have demonstrated that much larger, at least microscale-sized, pores are needed to model the Li-PS shuttling accurately [12]. Depending on the complexity of the model and the computational power at hand, it could take several days to run a single simulation [59], hindering comprehensive and systematic evaluation of possible electrode structures, dopants, electrolytes, and electrocatalysts.

Secondly, many experimental studies focus on the effects of dopants and electrocatalysts; however, there are not enough measured parameters for the DFT modeling. The addition of the dopants and electrocatalysts requires additional parameters such as differential charge density [65], which frequently lack experimentally derived values [12]. This diminishes the ability of these models to provide insights into electrode design and the predicted behavior associated with various electrode structures, chemistries, and electrocatalysts.

Thirdly, the physical phenomena in Li/S batteries, such as absorption, diffusion, and reaction, require unique simulation designs. Currently, researchers must manually select the appropriate exchange–correlation functional based on the complexity of the model such that the simulation results may be considered accurate, which requires considerable time, knowledge, and skill [59,60].

Finally, current DFT models assume ideal operating conditions and constant volume [59], neglecting more realistic working environments such as elevated temperatures and pressures and the associated time-dependent phenomena such as evolving volume [79] and reaction kinetics [80]. These assumptions originate from the fact that DFT models alone are incapable of accounting for time-dependent phenomena such as the breakdown of electrolyte molecules and product precipitation. By utilizing AIMD models within the framework of DFT models, some time-dependent phenomena can be elucidated at the expense of additional computational burden and simulation time [12,60].

### 2.1.3. Perspective

Due to the inherent limitations of DFT and AIMD models, the predictive capabilities of atomic-scale models in the context of Li/S batteries remain primarily limited to the verification and explanation of experimental findings [12]. However, DFT/AIMD simulations have provided useful insights for rational design [13], including Li-PS binding properties of potential electrode structures [65,68–72,74], dopants [34,65–67], and electrocatalysts [68,69,73,77,78]. Furthermore, these models have been used to elucidate the impact of electrolyte chemistry on the structure and behavior of Li-PS in solution [64] and to describe reaction phenomena occurring at the electrodes during lithiation and delithiation [61–63]. A comprehensive analysis of Li-PS binding through chemical and mechanical properties at the cathode may help researchers improve cycle life by confining the Li-PS shuttle effect to the cathode.

Additional approaches must be developed to improve model accuracy such that volume evolution over time and non-ideal operating conditions can be accounted for more efficiently. Moreover, as model complexity increases, additional parameters will be introduced inherently, and more sophisticated exchange–correlation functionals must be developed. Therefore, parameterizing solutions must be considered in tandem, such as developing and implementing machine learning (ML) techniques to quickly parameterize

models [81,82] and evaluate their efficacy [83]. ML techniques may also prove useful in developing novel exchange–correlation functionals [84]. Furthermore, the computational demand of DFT models is exponentially proportional to the model complexity. Therefore, the computational power available to researchers must simultaneously improve, in order to include time-dependent phenomena occurring over a greater spatial domain.

## 2.2. Molecular Dynamics

Molecular dynamics (MD) is a modeling technique based on analytical and statistical mechanics [85]. Unlike AIMD, MD does not intrinsically consider many-body effects such as bonding, charge transfer, and polarization. Instead, these effects are simplified to interatomic potential functions or force fields, dramatically reducing the computational burden. This allows MD models to make predictions at the mesoscale. The technique is adaptable based on the complexity of the model, ranging from structureless molecules that require only Newtonian mechanics to complex molecules with many degrees of freedom, which require Euler equations, Hamilton’s quaternions, and Lagrange methods [85]. MD simulations have primarily been used to elucidate the physical structures of active materials, material properties, and their dependence on electrolytes and the state of the cell [86–90].

### 2.2.1. Application

Like DFT models, MD simulations have been useful in evaluating properties critical to species transport and the Li-PS shuttle phenomenon. To analyze the structure, dynamics, and consequent properties of various electrolytes and solvated electrolytes, Park et al. developed an MD electronic continuum model tailored to state-of-the-art electrolyte–solvent systems for Li/S batteries [91], including lithium-bis(trifluoromethane)sulfonimide (LiTFSI) and lithium nitrate ( $\text{LiNO}_3$ ) in organic solvent mixtures of 1,2-dimethoxyethane (DME) and 1,3-dioxolane (DOL) [86]. The model allowed the researchers to evaluate the composition of the first lithium solvation shell [92], the temperature dependence of lithium diffusion, transference numbers, and the ionic and electrical conductivity of the considered electrolyte–solvent solutions [86]. Similarly, S. Han et al. used an MD model to evaluate the solvent exchange dynamics of the lithium solvation shell of a nonaqueous electrolyte, lithium hexafluorophosphate ( $\text{LiPF}_6$ ), as a function of the solvent mixture ratio [87]. K.S. Han et al. used MD to evaluate the diffusivity of several electrolyte anions, including bis(fluorosulfonyl)-imide ( $\text{FSI}^-$ ), triflate ( $\text{TFO}^-$ ), bis(trifluoromethanesulfonyl)-imide ( $\text{TFSI}^-$ ), and 2-trifluoromethyl-4,5-dicyanoimidazole (TDI $^-$ ). In doing so, they were able to describe ion–ion and ion–solvent interactions to show a relationship between anion mobility and the formation of thicker passivation layers at the lithium electrode due to undesired side reactions [88]. More recently, Babar et al. used MD to evaluate ion dimensions of the electrolyte and Li-PS in solvated and desolvated states (see Figure 2). These values were then used to determine the diffusion coefficient, rate of transport, and desolvation energy of each species [89]. MD simulations have also been used to evaluate various nanoscale sulfur electrode structures; Li et al. applied the technique to assess the performance and properties of several sulfur-doped carbon nanoparticle designs. Using the model, they were able to determine the thermodynamic stability of the sulfur electrode structure and the speciation and distribution of Li-PS within the nanoparticles [90].

### 2.2.2. Challenges

Like DFT simulations, MD models are limited in providing insights useful to rational design for a few reasons. Firstly, due to the high computational cost of MD, the simulations are constrained to small temporal and spatial scales, of the order of several hundred molecules over tens of nanoseconds [85,87,90]. Furthermore, depending on the complexity and number of molecules in the model, it can take days to complete a single simulation [85]. This hinders systematic studies and the scope of the phenomena that can be considered, because MD simulations often have to run multiple times to adequately sample potential initial conditions and consequent observations [12,85]. Moreover, because

of the computational cost, MD simulations simplify the structures, forces, and mechanics involved in order to make predictions; however, the actual electrochemical phenomenon in the Li/S system is much more complex [79,80,85].

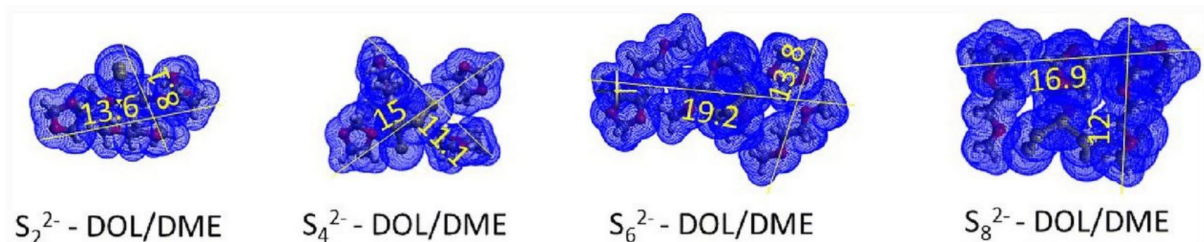


**Figure 2.** 3-D molecular models of solvated intermediate polysulfide anions including Van Der Waals surfaces. Electrolyte solution is LiTFSI in DOL/DME with dimensions measured in angstroms [89]. Produced by Babar, S. and Lekakou, C., licensed under CC BY 4.0.

Secondly, models are typically validated and parameterized using experimental findings; however, there is the fundamental challenge of determining whether the assumptions made regarding the structure, forces, and interactions considered in the model can be regarded as valid in practice [12]. This has been prohibitively tricky because of the inherent difficulty of *in situ* characterization [93] and the unique multi-step solid–liquid–solid reaction route [80].

Finally, current MD models that account for electrode structure assume that the sulfur electrode has constant and uniform pore sizes [89,90], which are typically measured by gas adsorption tests [94] or X-ray nano-computed tomography (CT) [95]. However, real sulfur electrodes have a heterogeneous pore size distribution. Moreover, the nonuniform structure experiences significant mechanical stresses as the volume changes by up to 80% during cycling [35,96], but these critical features have been neglected [89,90]. Consequently, some of the predictions made by MD simulations may not be accurate in practice and therefore must be experimentally validated.

### 2.2.3. Perspective

MD models have proven useful in evaluating species transport properties and parameters associated with solvated polysulfides and electrolyte anions. These include diffusivity [86–89], conductivity [86], transference numbers [86], exchange dynamics [86,87], and desolvation energy [89]. They have also been used to evaluate speciation and distribution within cathode structures [90]. This information may be useful in developing novel materials, cathodes, and separators to improve cycle life by inhibiting the Li-PS shuttle effect. As more methods to experimentally validate MD become available, the models can evaluate the cell-level material properties and phenomena that can help develop larger-scale, physics-based electrochemical continuum models. Specifically, this includes reaction kinetics models that detail the multi-step reaction process, and deposition models that describe solid-product ( $S_8$  and  $Li_2S$ ) precipitation on the sulfur electrode microstructure. Such models could be used to elucidate the deposition kinetics during cycling and to determine electrochemical parameters associated with novel electrolytes, solvated electrolyte ions, and solvated Li-PS [12].

Some of the remaining challenges associated with applying MD simulations to Li/S batteries may be overcome with the recent progress in *in situ* optical spectroscopic techniques, which include Raman, infrared, and ultraviolet spectroscopies [93,97,98]. These techniques may be used to develop the spatial domains, allowing researchers to characterize the highly heterogeneous and evolving cathode structure [86,90], as well as the complex multi-step reaction mechanisms [99]. ML may also contribute to solving the remaining challenges by improving the accuracy of MD simulations. This can be accomplished by replacing classical force fields with more accurate force calculations that utilize quantum mechanical DFT data to simulate force interactions at larger scales [100]. Similarly, ML can

be used to analyze MD simulation data and efficiently sample underlying free energy surfaces and kinetics [101]. Simultaneously, as computational power continues to increase and new computing methods become available, MD simulations will be capable of reflecting increasingly complex molecular-scale phenomena [85].

### 2.3. Continuum Models

Due to advances in computing power and *in situ* characterization techniques [93,97,98], high-fidelity physics-based continuum models are becoming increasingly feasible. Unlike DFT and MD-based models, continuum models describe macroscale electrode and cell-level phenomena. These models can be used to evaluate varying time and volume scales from 0D to 3D, thereby accurately capturing the effects of sophisticated chemical, electrochemical, and transport phenomena occurring within a Li/S cell. There are several approaches to developing these models, which are based on well-established mesoscale LiB modeling methods [12,102], the particle-based lattice Boltzmann method (LBM) [103], and direct numerical simulation (DNS)-based computational fluid dynamics (CFD) [104]. LBM is used to evaluate pore-scale transport equations on a pixel-level lattice. Complex physical phenomena occurring within the highly heterogeneous sulfur electrode structure can be resolved at a high resolution. Alternatively, the DNS-based CFD approach is used to evaluate the governing partial differential equations of transport in the porous sulfur electrode structure [12]. Continuum models have been used at pore and electrode scales to understand the relationship between material properties and battery performance and to understand species transport, identify limiting factors, and provide insights on mitigating strategies to improve cycle life [12].

#### 2.3.1. Application

Based on the work of Kumaresan et al. [105], Zhang and Marinescu et al. developed a series of 0D models that account for the effect of concentration-dependent electrolyte conductivity as a function of precipitation by relating it to the state of charge. However, the models still do not capture the effects of localized mass and charge transport, thereby inhibiting the ability to predict transport limitations [106–108]. To provide insight into the Li-PS shuttle effect, Mikhaylik and Akridge developed a thermally coupled lumped parameter 0D model to evaluate the effect of the PS shuttle phenomenon during cycling by applying the Nernst equation and assuming a simplified two-stage reduction reaction [44]. Similarly, Hua et al. applied differential thermal voltammetry to develop a 0D thermally coupled electrochemical Li/S model capable of describing the charge rate and temperature dependence of the Li-PS shuttle effect in real-time [109]. Likewise, Hofmann et al. built a 1D continuum model focused on describing the capacity loss and voltage drop induced by the Li-PS shuttle effect during cycling; their model was consistent with experimental observations [46]. In earlier work, Kumaresan et al. attempted to capture the intrinsic changes in porosity and electrochemically active sulfur area during cycling by proposing a 1D model based on the Nernst–Planck equation for dilute species [105]. However, a sensitivity analysis of Kumaresan’s model completed by Ghaznavi et al. highlighted the importance of experimental validation of the morphological parameters assumed in their work, due to a lack of reference values [110].

To evaluate optimal structural and electrolyte properties, Danner et al. implemented a 1D multiscale model (MSM) tailored to cathodes consisting of mesoporous and microporous particles. In their work, they were able to improve the simulated cycle life by using solvent systems with low PS solubility or high salt concentrations [111]. To observe passivation layer growth due to  $\text{Li}_2\text{S}$  precipitation, Thangavel et al. developed a similar multiscale 1D dual pore model tailored to a porous-particle-coated sulfur matrix that accounted for macropore and mesopore interparticle structure, electrochemical reaction kinetics, and ion transport. Their objective was to evaluate the reproducibility of predicted discharge trends, namely, the faster precipitation of  $\text{Li}_2\text{S}$  as well as the accelerated blocking of the interpores and mesopores nearest the separator [112]. In similar work, Ren et al. built a 1D model to

evaluate the impact of Li<sub>2</sub>S nucleation and growth on discharge behavior. They were able to show that by promoting uniform growth by providing nucleation sites and lowering nucleation rate, cycle life and discharge capacity could be improved [113].

More recently, Wen et al. developed an experimentally validated 1D cell-scale model that details the multiphasic reactions during self-discharge of Li/S batteries as a function of depth of discharge. The model can describe the reversible and irreversible capacity losses resulting from shuttling and precipitation at the lithium electrode [114]. Andrei et al. developed a 1D rate-dependent nucleation model to observe the dependence of Li/S battery capacity on discharge rate. The model is based on a modified Kolmogorov–Avrami model [115], which expresses the nucleation rate of solid products in terms of surface oversaturation of the precipitate [116]. Similarly, Danner et al. developed a 1D continuum model based on the classical theory of nucleation and growth [117,118]. Using an evolving particle size distribution of Li<sub>2</sub>S and S<sub>8</sub>, their model described the particle morphology and its effect on active surface area and species transport [118]. In similar work, Xiong et al. built a 1D transient model focused on the charging process of Li/S batteries. Specifically, their model was focused on elucidating the dependence of Li<sub>2</sub>S particle size on dissolution rate. They were able to show that the dissolution rate of larger Li<sub>2</sub>S particles was suppressed at lower potential due to the low specific surface area, while smaller Li<sub>2</sub>S particles were quickly electrochemically oxidized into dissolved PSs. They also observed that the dissolved PSs acted as redox mediators to accelerate the oxidation of larger Li<sub>2</sub>S particles [119].

To more accurately account for the evolution of the multiscale ( $\mu\text{m}$ –nm) heterogeneous cathode structure and its impact on the Li-PS shuttle effect, Lu et al. combined CFD with X-ray CT and morphological operation to evaluate the graded microstructure of a lithium electrode. The technique accurately modeled the performance of a LiB utilizing a 3D nano-microstructure electrode [102]. Tan et al. conducted similar 3D and 4D image-based investigations, combining micro and nano X-ray CT to derive several spatial effective transport parameters of a Li/S electrode, including sulfur distribution, conductivity, diffusivity, and porosity [120,121]. To elucidate the impact of surface passivation and blocked pores due to the precipitation of Li<sub>2</sub>S, Thangavel et al. developed a novel 3D kinetic Monte Carlo simulation based on a variable step-size method to evaluate the microstructural evolution due to precipitation, dissolution, and diffusion of individual PS species. They were able to show a relationship between S<sub>8</sub> loading and pore blockage, indicating that as initial sulfur loading increases, discharge capacity may decrease if pore blockage is not addressed simultaneously [122]. Similarly, using a 3D mesoscale model based on the finite volume method (FVM), Mistry et al. determined that surface passivation and pore blockage due to precipitation morphology contribute significantly to microstructural evolution, cell performance, and degradation [123]. To overcome the computational limitation of high-resolution 2D and 3D models, Agnaou et al. developed a novel technique called pore-network modeling (PNM), capable of describing the transport of charged species through pore networks by coupling the Nernst–Planck equations with fluid flow and charge conservation. This approach simplifies the complex pore microstructure into a pore–throat–pore network of either rectangles and circles for 2D or cylinders and spheres for 3D models (see Figure 3a,b). This significantly reduces computational demand with relatively minimal impact on model accuracy: less than 5% deviation compared to traditional finite element methods (FEM) [124].

### 2.3.2. Challenges

Several challenges still hinder the development of higher-order electrode-scale models, thus limiting their application to rational design and novel solutions. Firstly, DNS-based CFD models are computationally taxing. The computational demand of these models is exponentially proportional to the size of the domain; pore-scale models can take several hours to complete a single simulation [90], while electrode-scale models can take multiple

days [112]. Furthermore, computational demand increases as the number of dimensions is increased from lumped parameter 0D models to 3D continuum models.

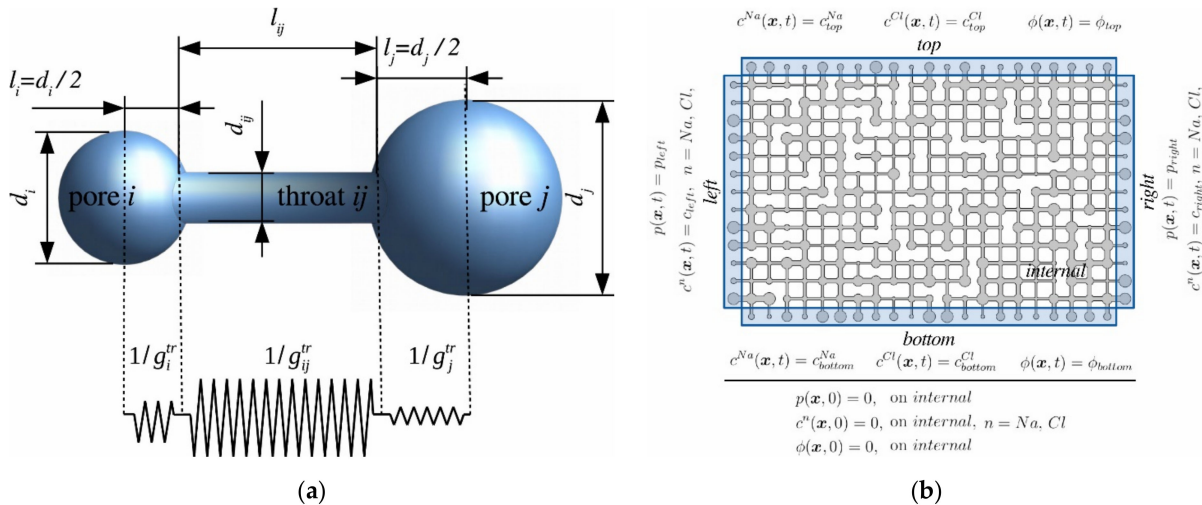


**Figure 3.** Diagram of (a) individual and (b) combined pore-throat-pore nodes. Each conduit consists of a throat, and half of each adjacent pore. Transport is described by size dependent resistance in series. The size and spacing of each pore is random [124]. Reprinted from Computers & Geosciences, Vol. 140, Agnaou, M.; Sadeghi, M.A.; Tranter, T.G.; Gostick, J.T. Modeling Transport of Charged Species in Pore Networks: Solution of the Nernst–Planck Equations Coupled with Fluid Flow and Charge Conservation Equations, pages No. 3–7, Copyright 2020, with permission from Elsevier.

Secondly, current mechanistic models are based on the Bruggeman correlation between tortuosity and porosity. However, this approach assumes uniform porosity distribution of a highly heterogeneous sulfur electrode morphology, thereby neglecting the effect on species transport [125]. Moreover, existing physics-based electrochemical models describe the transport of active materials using Kumaresan’s dilute solution theory [105]. However, experimental findings have shown that optimized Li/S cells contain high concentrations of sulfur [17], with an electrolyte-volume-to-sulfur-weight (E/S) ratio of less than 3 or 4 [12,126].

Thirdly, the morphological changes resulting from PS precipitation and dissolution alter the spatiotemporal microstructural parameters such as the electrical conductivity, active surface area, and porosity. Adapting physics-based electrochemical models to account for these factors is computationally expensive and challenging to experimentally validate [112]. In addition, characterization of the highly heterogeneous sulfur electrode structure is necessary, as it plays a role in species transport, electrochemical potentials, electrolyte resistance, and electrode durability [79]. However, current continuum models themselves are unable to adequately represent this structure, thereby requiring additional *in situ* visualization techniques [127], which themselves have proven challenging to develop [93].

Finally, because of the difficulty involved in producing and isolating individual Li-PS species from other complexes, radicals, and additives [79,128], there is a lack of experimental analysis of the thermodynamic properties of Li-PS, thereby hindering the physical representation of cell performance, as the values must be assumed or parameterized [12]. Hence, the models discussed in this section qualitatively predict the discharge curve at various discharge/charge rates; however, they do not reflect experimentally validated spatiotemporal parameters such as depth of discharge behavior, activation polarization, and electrolyte resistance. Furthermore, a standard for phenomena and mechanisms to include in future model iterations has not yet been determined because their impact on cell behavior has not yet been established [12]. Due to the computationally taxing nature of continuum modeling, researchers must carefully select which physical, chemical, and electrochemical mechanisms to include. However, there is no consensus regarding which

mechanism most accurately reflects the real conditions such that the simulated results may be useful in elucidating limiting factors and guiding future development.

### 2.3.3. Perspective

Continuum simulations have proven useful in elucidating the Li-PS shuttle phenomenon [44,46,102,109,114], characterizing precipitation-dependent cathode evolution [105,112–114,116,118,122,123], and identifying key design considerations for cell performance [106–108,111,113,119–121]. The continued development of electrode and cell-scale continuum models will allow researchers to extract physical parameters from experimental data, optimize cell design for specific applications, simulate proposed solutions, and direct their focus to areas that offer an efficient means of improving cell performance.

Several challenges and limitations remain inherent to modeling electrochemical and physical phenomena at larger macroscales, particularly given the complex nature of Li/S reaction mechanisms; however, researchers have made several advancements to alleviate these challenges in recent years. Though the technique has not yet been applied in the context of Li/S batteries, PNM are a promising method for efficiently elucidating mesoscale phenomena [124]. Furthermore, advanced visualization techniques such as X-ray CT scans [102,120,121] and Raman spectroscopy may be combined with high-fidelity 3D continuum models to describe structural evolution during cycling [97,98]. To balance model accuracy and computational expense, Kulkarni et al. suggest combining electrochemical modeling, including particle-scale DNS models and electrode-scale PNMs, with electrode morphology generated using *in situ*/operando visualization techniques. However, it simultaneously introduces a degree of uncertainty/errors which arise from phase segmentation [12].

Alternatively, ongoing advancements in computing power make it increasingly feasible to develop MSMs that implement DFT and MD simulations at scales associated with continuum models. Such models are of particular interest in Li/S battery development and may be useful in elucidating the transport phenomena and reaction kinetics that occur at micro and mesoscales within the porous cathode structure. However, local singularities, grid convergence, boundary layers, and moving boundaries must be given careful attention [129]. Traditionally, MSMs have sequentially simulated each process and combined them through coupling; however, this approach is computationally taxing, suffers from phase segmentation errors, and produces unsatisfactory coupling of some phenomena [130]. ML may be the key to unlocking the full potential of MSMs. They could be used to couple multiscale simulations, accelerate model development, and ensure experimental validity [131]. Recently, Kolodziejczyk et al. demonstrated the effectiveness of ML in MSM development. Their team built an MSM based on FEM to evaluate the thermal properties of composite phase change materials and develop a thermal management system for LiBs. Their results demonstrated excellent accuracy when compared to traditional FEM models, with a maximum temperature difference less than 0.005% and 0.015% over discharge [132]. ML may also be helpful in guiding future model development by identifying critical performance factors and systematically analyzing materials and electrolytes for properties which may satisfy them [133]. They may also be used to improve the speed and accuracy of visualization techniques to characterize cathode structures and speciation [134].

### 2.4. Modeling and Manufacturing

Manufacturing of Li/S cells is, of course, a key consideration in commercializing the technology. Electrochemical modeling may also prove useful in elucidating the impact of manufacturing procedures on battery performance properties. Danner et al. developed a continuum model consisting of a particle scale model coupled to a macroscopic cell model. Using the model, they were able to evaluate the relationship between cell performance and production parameters for sulfur-impregnated microporous carbon particles [111]. Specifically, they considered increasing the inhomogeneity of the sulfur within the particle, which has been shown to be related to production temperature and pressure [135]. In

similar work, Liu et al. built a pair of DFT and 1D FVM-based models to evaluate the in situ fabrication of an acrylate-based hierarchical electrolyte and its effectiveness in inhibiting the Li-PS shuttle phenomenon. They showed that by altering gelation and electrospinning duration, the thickness of AHE can be controlled and optimized to inhibit the shuttle effect and minimize ohmic polarization [136]. In more recent work, Feng et al. attempted to establish procedures for rational design, scalable fabrication, and characterization of high-quality thick sulfur cathodes. They proposed an active material microenvironment model to elucidate the role of the calendaring process on electrode quality. They showed that the calendaring process could alter the electrochemical performance of the cell by decreasing the volume fraction of mesopores and micropores, as well as reshaping and stabilizing the microstructures of the ion and electron transport network [137].

Manufacturing models for Li/S cells may also draw inspiration from existing methodologies used in LiB production. Thomitzek et al. developed a holistic multi-level simulation combining process chain and cell-scale electrochemical models to evaluate the impact of varying process controls on structural and electrochemical parameter distribution, as well as resultant battery performance properties [138]. The simulation-based approach details the interdependencies of quality parameters along the process chain, characterizes the completed cell, and predicts investment and operational expenses. The simulation may also be used to identify sensitive process parameters and estimate the impact of manufacturing tolerances on electrochemical properties. In a later case study, they demonstrate model efficacy by determining whether mean manufacturing parameters achieve optimal cell performance and by quantifying the impact of uncertainty propagation in manufacturing on electrochemical performance [139]. In related work, Ngangjong et al. endeavored to produce a digital twin of the complete LiB manufacturing process. They produced a 3D discrete element method (DEM)-based calendaring model which considered both active material and carbon binder domains. They paired their model with two existing models, a coarse-grained MD model to detail slurry equilibration and drying and a 4D FEM-based model to simulate cell performance. Using the model, they elucidated the relationships between the electrode mesostructure, cell performance, and calendaring pressure for a  $\text{LiNi}_{0.33}\text{Mn}_{0.33}\text{Co}_{0.33}\text{O}_2$  cathode. They plan to adapt the model to include alternative particle shapes and chemistries, then use it to evaluate the impact of additional calendaring parameters such as temperature and pressure on cell performance [140]. Similar holistic models for Li/S batteries are lacking in the literature and may be a potential research avenue to accelerate commercialization.

### 3. Challenges in the Design and Development of Li/S Cell Components

#### 3.1. Sulfur Electrode Design Challenges

The major technical challenges of Li/S cells discussed in the introduction section are mainly associated with the sulfur electrode. Although the sulfur electrode can theoretically deliver a very high specific capacity of  $1675 \text{ mA h gS}^{-1}$ , the practical utilization of sulfur is still not satisfactory (generally <60%) and the long-term cyclability and power density are not yet compatible with those of Li-ion cells. The problematic Li-PS shuttle causes the loss of active sulfur and the deposition of  $\text{Li}_2\text{S}$  onto the lithium electrode, resulting in cell capacity degradation. Inhomogeneous reconfiguration of the sulfur electrode microstructure due to the uncontrolled Li-PS formation and the volume changes of sulfur particles is another concern for the design of sulfur electrodes. On the other hand, Li-PS is also considered essential for Li/S-cell operation because it provides the sulfur electrodes with a kinetically fast route for reaction with lithium ions [141]. The solution-based pathway involving Li-PS can overcome the large energy barrier for the charge transfer reaction at the sulfur/electrolyte interface and Li-ion diffusion through solid sulfur particles. Ideally, sulfur electrodes should prohibit the Li-PS shuttle while allowing homogeneous Li-PS formation and deposition back to the sulfur electrode as sulfur or  $\text{Li}_2\text{S}$ .

The sulfur–carbon composite is the most popular active material design for improving the sulfur electrode's capacity and cyclability by mitigating the Li-PS shuttle effect. Various

carbonaceous materials such as porous carbons, 1D carbons (carbon nanotubes, carbon nanofibers), and 2D carbons (graphene and graphene oxide) have been investigated as sulfur host materials or functional additives for sulfur electrodes to utilize their excellent electronic conductivity and good mechanical strength. Some carbonaceous materials have high sulfur-philic properties, which can mitigate the Li-PS shuttle phenomenon, resulting in improved cyclability [12,14,53,142–144]. Sulfur electrodes are manufactured by the slurry-based tape casting process like Li-ion cell electrodes, but the sulfur electrodes reported in research papers generally contain a large amount of carbon, at least 10–20 wt.% or sometimes even more than 50 wt.% (including the carbon in sulfur–carbon composite active material), to sufficiently mitigate the problems of the sulfur electrodes [14].

The large quantity of porous carbons often severely affects the slurry quality because carbons tend to aggregate with each other or absorb too much solvent in a slurry, making the slurry less flowable or inhomogeneous. In addition, the extremely low powder density of these carbons (e.g., Super P:  $0.16 \text{ g cm}^{-3}$ , Ketjen black:  $0.1 \text{ g cm}^{-3}$ ) tends to increase the sulfur electrode's thickness compared to that of the Li-ion-cell positive electrode. Casting a poorly prepared slurry often results in inhomogeneous thickness distribution, pinholes, or even delamination during the drying process. Increasing the binder content may help mitigate the mechanical damage, but it increases the 'dead weight' of the sulfur electrode. These issues will become more formidable as higher sulfur mass loading is required to achieve high specific energy. Therefore, more systematic design strategies are needed to design high-mass-loading sulfur electrodes. To develop thick and large-area sulfur electrodes for high energy Li/S pouch cells, functional materials or electrode fabrication parameters previously evaluated in small laboratory-scale research will need to be revisited and reoptimized.

For Li/S pouch cells to succeed in the electric transportation battery market, we anticipate that a high specific energy of  $>300 \text{ W h kg}^{-1}$  is required. Design calculation of the obtainable specific energy ( $\text{W h kg}^{-1}$ ) for a Li/S pouch cell is helpful to predict the essential design parameters of Li/S pouch cells. In particular, we evaluated the effect of sulfur mass loading, sulfur content, E/S ratio, and sulfur utilization (equivalent to the specific capacity of the sulfur electrode) on the obtainable specific energy of Li/S pouch cells. The passive weight values of pouch cell components listed in Table 1 were used for the design calculations. Figure 4a shows the specific energy of the Li/S pouch cell for various sulfur mass loadings and E/S ratios. The results indicate that a specific energy of  $>300 \text{ W h kg}^{-1}$  requires a high sulfur mass loading of  $>\sim 6 \text{ mg cm}^{-2}$  and a low E/S ratio of  $\leq 4$  while achieving  $>70\%$  sulfur utilization ( $1172.5 \text{ mA h gS}^{-1}$ ). A Li/S pouch cell with an E/S ratio of higher than six is unlikely to show the desired specific energy, no matter what the sulfur mass loading, unless significantly higher sulfur utilization (80–90%) is achieved. Figure 4b shows the variation of the obtainable specific energy for various sulfur utilization and sulfur mass loading values at a fixed E/S ratio of 3. The results (Figure 4b) indicate that sulfur utilization plays a critical role in achieving a high specific energy of  $>300 \text{ W h kg}^{-1}$ . The 50% utilization is still mandated even with a very high sulfur loading of  $20 \text{ mg cm}^{-2}$  and a low E/S ratio of 3. According to the design calculations shown in Figure 4a,b, targeting the following electrode fabrication parameters is reasonable for delivering a specific energy of  $300 \text{ W h kg}^{-1}$ : a sulfur loading of  $\geq 6 \text{ mg cm}^{-2}$ , a sulfur utilization of  $\geq 70\%$ , and an E/S ratio of  $\leq 4$ . The design parameters become more challenging for a higher specific energy of  $400 \text{ W h kg}^{-1}$ : a sulfur loading of  $\geq 10 \text{ mg cm}^{-2}$ , a sulfur utilization of  $\geq 80\%$ , and an E/S ratio of  $\leq 3$ . Unfortunately, a low E/S ratio of  $\leq 4$  often results in low sulfur utilization [145] or poor cyclability [146] as it results in a slow electrochemical process at the sulfur electrode (e.g., low Li-PS solubility, electrolyte decomposition) [147,148].

**Table 1.** Approximate values for the pouch cell components. A double-side coated sulfur electrode and lithium electrode were considered.

	Component	Weight
Current collectors	Aluminum foil for sulfur electrode	4.05 mg cm <sup>-2</sup>
	Copper foil for lithium electrode	8.96 mg cm <sup>-2</sup>
	Lithium Metal	1.5 × theoretical relative to S loading
	Separator (porosity 55%)	1.035 mg cm <sup>-2</sup>
Pouch materials	Tab-negative electrode	221.9 mg
	Tab-positive electrode	76.4 mg
	Pouch laminate	75.6 mg cm <sup>-2</sup>
	Unit electrode area	20 cm <sup>2</sup>
The number of lithium electrodes (or sulfur electrodes)		10
Electrolyte density		1
Li/S cell operating voltage		2.15 V

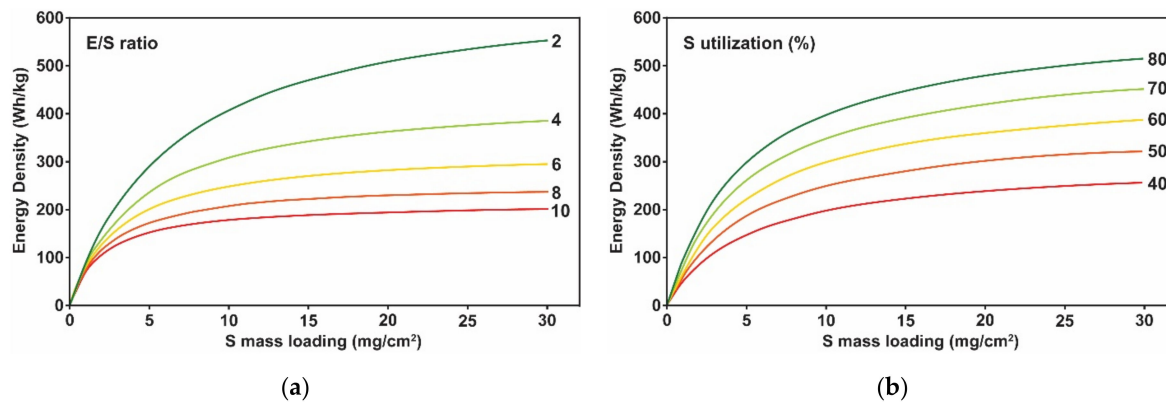


**Figure 4.** Design calculation of Lithium-Sulfur (Li/S) pouch cell specific energy (a) Obtainable specific energy for various sulfur mass loading and electrolyte/sulfur (E/S) ratios. Sulfur content and sulfur utilization were fixed to 80% and 70%, respectively. (b) Obtainable specific energy for various sulfur loading and sulfur utilization. E/S ratio and sulfur content were fixed to 3 and 80%, respectively.

A low E/S ratio of 3–4 with reasonable specific capacity ( $1000\text{--}1200 \text{ mA h gS}^{-1}$ ) has recently been reported via chemical or morphological modification of sulfur electrodes [149–152]. Although the capacity retentions were not sufficient for commercialization, the authors' accomplishments in successfully reducing the E/S ratio emphasize the importance of the sulfur electrode design. However, in most research studies, the electrolyte amount was adjusted to achieve the target E/S ratio, regardless of the electrode's design parameters such as porosity and sulfur content. In principle, however, the pore volume and the electrode surface area generally determine the required amount of the liquid electrolyte, since the pores of the sulfur electrode are supposed to be filled by the liquid electrolyte to form a continuous ionic percolation network and an adequate electrochemical interface. Li/S cells suffer from either electrolyte shortage or excess if the electrolyte amount is determined without considering these parameters.

For this reason, we performed additional design calculations for the Li/S pouch cell to reflect the correlation between porosity, sulfur content, and the E/S ratio. We assumed that the required electrolyte volume was the same as the total pore volume of the sulfur electrode and a separator, with no excess added. The design calculation results shown in Figure 5a,b indicate that the porosity of the sulfur electrode plays a critical role in determining the obtainable specific energy because the E/S ratio increases as the porosity of the electrode increases. We previously stated that a sulfur mass loading of  $>6 \text{ mg cm}^{-2}$  would provide an opportunity to achieve  $300 \text{ W h kg}^{-1}$  when the E/S ratio is  $\leq 4$  and sulfur utilization is  $<70\%$  (Figure 4a). However, according to the design calculation, the low E/S ratio of  $\leq 4$  is unlikely to be achievable with a sulfur mass loading of  $6 \text{ mg/cm}^2$  and

sulfur content of 90%, unless the sulfur electrode has an extremely low electrode porosity of 10%. Based on the calculation results, we anticipate that porosity of about 3–40% with a sulfur mass loading of  $>10 \text{ mg cm}^{-2}$  would offer an excellent opportunity to achieve a high specific energy of  $>300 \text{ W h/kg}$ .

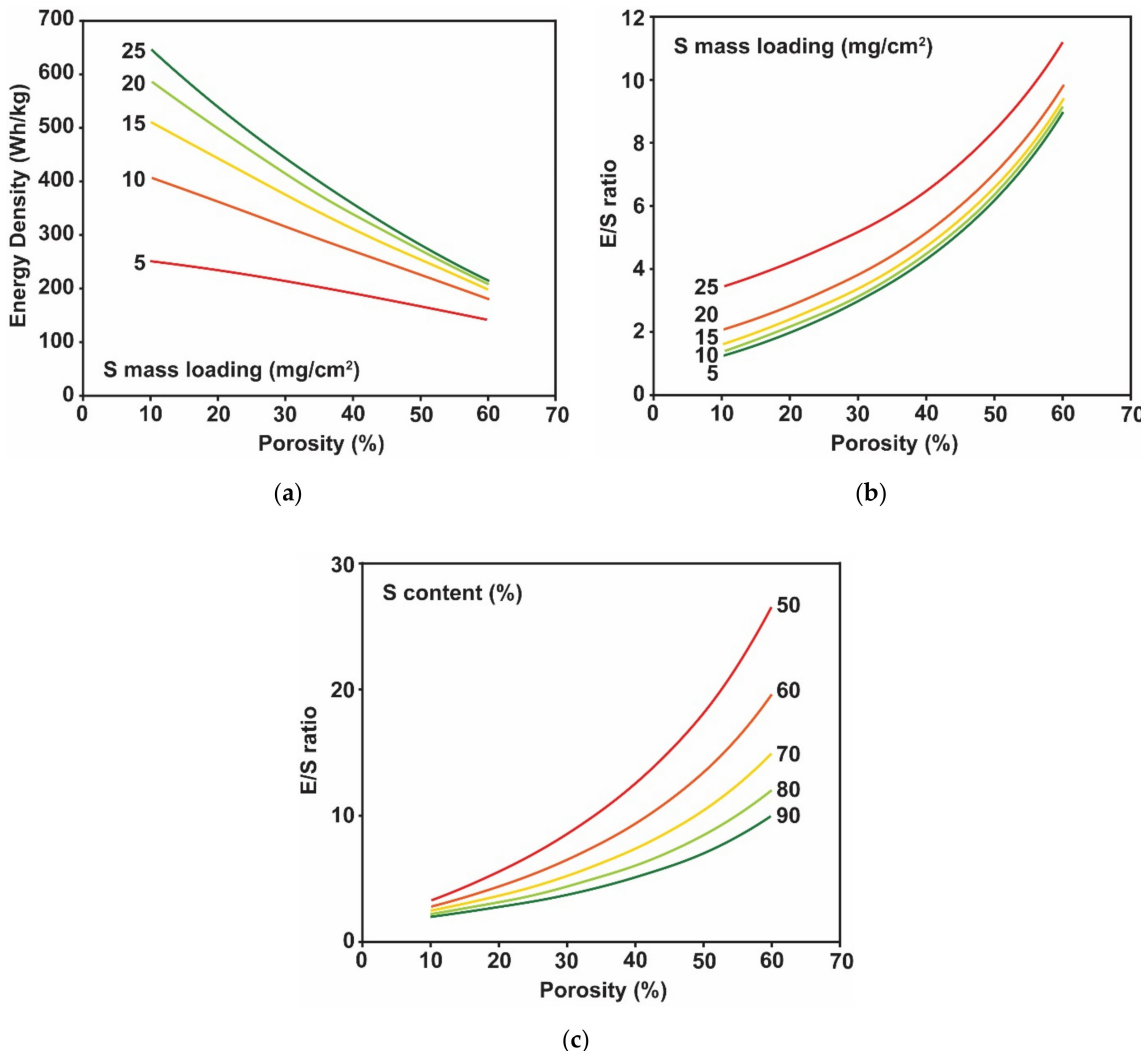


**Figure 5.** Design calculation results (a) Obtainable specific energy of a Li/S pouch cell for various porosity of sulfur electrode and sulfur mass loading. Sulfur content and sulfur utilization were assumed as 90% and 70%, respectively. (b) Variation in the E/S ratio depending on the sulfur electrode porosity and sulfur mass loading. The required electrolyte amount corresponds to the pore volume of the sulfur electrode and separator. The sulfur content was assumed as 90%. (c) Variation in the E/S ratio depending on the sulfur electrode porosity and sulfur content. Sulfur mass loading used for the calculation was  $10 \text{ mg cm}^{-2}$ .

The effect of electrode porosity raises another critical question about the influence of the sulfur content on the E/S ratio. The design calculations for the Li/S pouch cells shown in Figure 4 result in similar calculated specific energies of  $311 \text{ W h kg}^{-1}$  at a sulfur content of 50% and  $349 \text{ W h kg}^{-1}$  at a sulfur content of 90%, respectively (sulfur mass loading of  $10 \text{ mg cm}^{-2}$ , sulfur utilization of 70%, and an E/S ratio of 3). However, lowering the sulfur content of the sulfur electrode to add more carbon additives while maintaining sulfur mass loading significantly increases the thickness of the sulfur electrode. In other words, the total pore volume of the sulfur electrode is larger when the sulfur content is lowered, implying a higher E/S ratio for the Li/S cells. The design calculation results (Figure 5c) clearly show that the sulfur content affects the E/S ratio dramatically. According to the design calculation results, an E/S ratio of  $<~4$  for a sulfur mass loading of  $10 \text{ mg cm}^{-2}$  is only achievable

when the sulfur content is higher than 80% and the porosity is lower than 30% for the sulfur electrode. The calculated specific energies of the Li/S pouch cells (sulfur mass loading of  $10 \text{ mg cm}^{-2}$  and sulfur utilization of 70%) for sulfur content values of 50% and 90% are 184.6 and  $314.2 \text{ W h kg}^{-1}$ , respectively, which is obviously different from the calculated specific energy without consideration of porosity. The design calculation results emphasize that a high-sulfur-mass-loading electrode with a large quantity of carbon additive will not offer high specific energy even if high sulfur utilization is achieved. However, increasing the sulfur content can lower the sulfur utilization due to poor electronic conductivity [147]. Thus, adjusting the sulfur content must be considered thoroughly. Of course, the effect of electrode porosity can be mitigated if a carbon additive with a higher powder density is used or the powder density of carbon is increased by incorporating sulfur into the pores of the carbon.

### 3.2. Challenges in Lithium Metal Electrode

The lithium electrode has been investigated for high-energy lithium metal cells due to its high specific capacity and large negative potential ( $-3.06 \text{ vs. NHE}$ ). However, critical technical issues associated with the unstable lithium/electrolyte interface lead to concerns about the safety and reliability of Li/S cells. The repeated inhomogeneous stripping/plating processes or the formation of an unstable SEI during the cell operation causes lithium dendrite formation and growth, resulting in substantial performance degradation and cell failure [12,144,153–155]. In addition, the lithium metal electrode in the Li/S cell also suffers from the PS phenomenon. Until now, there have been various approaches to stabilizing the lithium/electrolyte interface, and these methods generally focus on the formation of a stable and ionically conductive SEI. However, despite the significant progress in improving the stability of lithium electrodes, the reliability of lithium metal electrodes is still not satisfactory for commercialization.

While enormous research efforts to stabilize the lithium metal electrode have already been made, we also need to address the challenges for Li/S cell manufacturing. According to the report by Park et al., an areal capacity of  $10 \text{ mA h cm}^{-2}$  results in repeated lithium stripping and plating of around  $50 \mu\text{m}$  in thickness [156]. This result implies that the lithium/electrolyte interface of the high-capacity Li/S cell will experience dramatic volume changes during cell operation. In addition, Li/S cells may require excessive lithium, generally 1.5–2 times more than the theoretical estimation, to prevent lithium depletion. However, the optimal lithium amount needs to be determined since excessive lithium increases the material cost and the weight of the Li/S cells. The high lithium metal cost due to the expensive thin-film engineering process is another potential problem for Li/S cell commercialization. According to a review article [157], the price for  $200 \mu\text{m}$  thickness lithium foil is about USD 100–300 per kg, whereas a  $20 \mu\text{m}$  thick lithium foil costs USD 250–1000 per kg. The author pointed out that using the thick lithium metal foil may provide an opportunity to omit a copper current collector, compensating for the cell weight increase, but the absence of a copper current collector may cause an electron conduction problem for the large-area Li/S pouch cell. Lithium-free electrodes such as carbon and silicon electrodes could be alternatives to resolve lithium-metal-related issues, but they significantly lower the specific energy of Li/S cells, and the use of a  $\text{Li}_2\text{S}$  electrode will be enforced, which will substantially increase the cell manufacturing cost.

### 3.3. Electrolyte Design Challenges

Li/S cells generally employ liquid organic electrolytes consisting of ether-based solvents, LiTFSI as a lithium salt, and  $\text{LiNO}_3$  as a functional additive. Tetraethylene glycol dimethyl ether (TEGDME) and a mixture of DOL and DME are the most widely used solvents among ether-based solvents. Ether-based solvents promote the Li-PS-based reaction route of sulfur electrodes, enabling a high sulfur utilization. Some other salts and solvents such as lithium perchlorate ( $\text{LiClO}_4$ ), lithium trifluoromethanesulfonate ( $\text{LiCF}_3\text{SO}_3$ ),  $\text{LiPF}_6$ , and carbonates-based solvents have also been investigated, but they are not as effective as

the conventional electrolyte systems. As discussed above, the Li-PS shuttle effect easily occurs in the absence of an effective barrier. LiNO<sub>3</sub> is an effective functional additive that mitigates the shuttle effect by forming a passivation layer on the lithium metal electrode, but recent studies indicate that LiNO<sub>3</sub> in the liquid electrolyte can increase the consumption of the active sulfur as a result of SEI formation on the sulfur electrode [158], or serve as a source of gas formation at approximately 40 °C [159].

Organic liquid electrolytes with high salt concentrations have been investigated as an alternative solution to mitigate the Li-PS shuttle effect. Several reports suggested that the high Li-ion concentration in electrolytes affects PS solubility due to the dissolution equilibrium principle. The results showed that the higher the lithium salt concentration, the lower the Li-PS solubility; hence, the Li-PS shuttle can be prevented, improving the cyclability of Li/S cells [160]. Similarly, adding ionic liquids to the ether-based electrolyte also improves the cyclability of sulfur electrodes by mitigating the Li-PS shuttle [127] or forming a passivation surface layer on a lithium metal electrode [161]. However, neither high-salt-concentration electrolytes nor ionic-liquid-containing electrolytes are feasible for commercialization because they often exhibit very high viscosity that causes a high voltage polarization or low power capability. In addition, LiTFSI and ionic liquids are still relatively expensive, so they are not economical options for Li/S cell manufacturing.

Solid electrolytes for solid-state Li/S cells have recently attracted attention because they can inhibit Li-PS formation and the shuttle effect due to the lack of liquid medium. In addition, the high mechanical strength of the solid electrolytes offers a better opportunity to suppress the internal cell shorting caused by lithium dendrite growth. Moreover, the wide thermal and electrochemical windows and non-flammable natures of the solid electrolytes can dramatically reduce the safety concerns regarding the Li/S cells. However, none of the research has demonstrated high-performance solid-state Li/S cells comparable to conventional Li/S cells. Unfortunately, solid-state Li/S cells have several technical problems at the lithium–solid electrolyte and the sulfur–solid electrolyte interfaces [162–164]. Furthermore, the solid-state interfacial electrochemistry of the Li/S solid-state cells is not fully understood; thus, intensive fundamental research is certainly required. Some studies showed improved sulfur utilization and cyclability, but their testing conditions are far from those of practical operation conditions (e.g., too low discharge cut-off voltage, high operation temperature, or low current for testing).

#### 3.4. Separator Design Challenges

Developing a polymer separator that can enhance the performance of Li/S cells is also essential because the separator can also directly impact the electrochemical behavior of Li/S cells. Polyethylene (PE) and polypropylene (PP) with the micrometer-sized pores common in LiBs [165] are also used in Li/S cells. More details on the separator technology are available in review articles [166,167]. The separator is one of the main contributors to the material cost for LiB manufacturing [168], and its weight and the electrolyte filling in its pores contributes to the weight of inactive components, implying that the separator design will be the critical factor determining the specific energy and energy cost of Li/S cells. For designing the Li/S cell separator, several things must be considered thoroughly: (1) the wettability towards ether-based electrolytes, (2) the thickness and porosity to minimize the inactive weight increase, (3) the thermal and mechanical stability, (4) the barrier functionality to prevent Li-PS shuttling, and (5) a low material price. Integration of a functional interlayer into the separator or chemical surface modification to existing PE or PP separators would also be effective. For substantial improvement of Li/S cell performance for commercialization, the above-mentioned design parameters must be considered while carefully investigating its compatibility with other cell components such as lithium and sulfur electrodes and the electrolyte.

#### 4. Summary and Outlook

This paper briefly reviews Li/S cell technology and discusses future research and development towards practical Li/S cells for electric transportation. Li/S cells have great potential for reducing the weight and manufacturing cost of rechargeable batteries, providing compelling market opportunities for the electrification of automotive vehicles such as passenger cars, medium and large vehicles, and aircraft, where the specific energy and cost of batteries are significant concerns. In the past decade, the performance of Li/S cells has been significantly improved, but further performance enhancement is still required in terms of specific energy ( $>400 \text{ W h kg}^{-1}$ ), long-term cyclability ( $>500$  cycles with  $>80\%$  capacity retention), and fast-charging capability ( $<15\text{--}30$  mins) for widespread commercialization.

Developing the rational design of a Li/S cell consisting of high sulfur mass loading and content, low E/S ratio, and minimized lithium excess is essential for commercializing Li/S cells successfully, as discussed in Section 3. In addition, the advancements made at the laboratory scale need to be translated into large-scale development. Cell design parameters that were relatively neglected may need to be revisited and reoptimized as charge- and mass-transport behaviors can be significantly affected by dimensional variations of the electrochemical interfaces. The rational design of cell configurations can be supported by predictive modeling efforts that offer insights into the advancement and the failure mechanisms of Li/S cells, accelerating practical Li/S cell development. The model-based cell configurations will need to be investigated in conjunction with optimal manufacturing parameters (e.g., sulfur mass loading, sulfur content, porosity, and E/S ratio) to maximize the opportunity to develop commercially attractive Li/S cells. For successful market penetration, developing a prototype Li/S cell that exhibits high specific energy, an extended cycle life, and improved rate capability will need to be followed by further investigations into the reliability of Li/S cells. To date, the evaluation of Li/S cell performance has generally been performed under very mild conditions, far from battery operation conditions in actual applications. The reliability of Li/S cells for various temperatures, voltage windows, humidities, and operation rates needs to be investigated. Additional research and development effort will be required to resolve any reliability issues demonstrated.

There is no doubt that Li/S technologies are in a strong position among the next-generation rechargeable batteries, but it is also true that the technology readiness level of Li/S cell technology is not comparable with that of LiBs. However, directly comparing the current state-of-the-art LiBs and Li/S batteries seems unfair, considering the enormous infrastructure for research and manufacturing of LiBs. Our society anticipates extraordinary demands for rechargeable batteries within ten years. We may need alternative energy storage options to be readily available, in order to be prepared for uncertainty in the LiB supply. Over the next ten years, Li/S technologies need to move from academic-oriented research to coordinated academia–industry development, in order for the technology readiness levels of Li/S battery technology to continue to improve.

**Author Contributions:** Conceptualization, S.U.K. and Y.H.; Investigation: C.M., S.U.K. and Y.H.; writing—original draft preparation, C.M., S.U.K. and Y.H.; writing—review and editing, Y.A., S.U.K. and Y.H. All authors have read and agreed to the published version of the manuscript.

**Funding:** This research received no external funding.

**Institutional Review Board Statement:** Not applicable.

**Informed Consent Statement:** Not applicable.

**Data Availability Statement:** The data presented in this study are available on request from the corresponding authors.

**Conflicts of Interest:** The authors declare no conflict of interest.

## References

1. The Paris Agreement | UNFCCC. Available online: <https://unfccc.int/process-and-meetings/the-paris-agreement/the-paris-agreement> (accessed on 23 August 2021).
2. Coronese, M.; Lamperti, F.; Keller, K.; Chiaromonte, F.; Roventini, A. Evidence for sharp increase in the economic damages of extreme natural disasters. *Proc. Natl. Acad. Sci. USA* **2019**, *116*, 21450–21455. [[CrossRef](#)]
3. Fan, Y.V.; Perry, S.; Klemeš, J.J.; Lee, C.T. A review on air emissions assessment: Transportation. *J. Clean. Prod.* **2018**, *194*, 673–684. [[CrossRef](#)]
4. Reddy, M.V.; Mauger, A.; Julien, C.M.; Paoletta, A.; Zaghib, K. Brief History of Early Lithium-Battery Development. *Materials* **2020**, *13*, 1884. [[CrossRef](#)] [[PubMed](#)]
5. Choi, S.; Wang, G. Advanced Lithium-Ion Batteries for Practical Applications: Technology, Development, and Future Perspectives. *Adv. Mater. Technol.* **2018**, *3*, 1700376. [[CrossRef](#)]
6. Vernardou, D. Progress and Challenges in Industrially Promising Chemical Vapour Deposition Processes for the Synthesis of Large-Area Metal Oxide Electrode Materials Designed for Aqueous Battery Systems. *Materials* **2021**, *14*, 4177. [[CrossRef](#)] [[PubMed](#)]
7. Thackeray, M.M.; Wolverton, C.; Isaacs, E.D. Electrical energy storage for transportation—Approaching the limits of, and going beyond, lithium-ion batteries. *Energy Environ. Sci.* **2012**, *5*, 7854–7863. [[CrossRef](#)]
8. Frey, H.C.; Kuo, P.-Y. Assessment of Potential Reduction in Greenhouse Gas (GHG) Emissions in Freight Transportation; Emission Inventory Conference: Raleigh, NC, USA, 2007; pp. 15–17.
9. Masias, A.; Marcicki, J.; Paxton, W.A. Opportunities and Challenges of Lithium Ion Batteries in Automotive Applications. *ACS Energy Lett.* **2021**, *6*, 621–630. [[CrossRef](#)]
10. Sripad, S.; Viswanathan, V. Performance Metrics Required of Next-Generation Batteries to Make a Practical Electric Semi Truck. *ACS Energy Lett.* **2017**, *2*, 1669–1673. [[CrossRef](#)]
11. Hasa, I.; Adelhelm, P.; Cao, G.; Mai, L. Batteries & Supercaps: Beyond Lithium-Ion Batteries. *Batter. Supercaps* **2021**, *4*, 1036–1038.
12. Robinson, J.; Xi, K.; Kumar, R.V.; Ferrari, A.C.; Au, H.; Titirici, M.-M.; Puerto, A.P.; Kucernak, A.; Fitch, S.D.S.; Garcia-Araez, N.; et al. 2021 Roadmap on Lithium Sulfur Batteries. *J. Phys. Energy* **2021**, *3*, 031501. [[CrossRef](#)]
13. Thompson, S.C.; Paredis, C.J.J. *An Introduction to Rational Design Theory*; American Society of Mechanical Engineers Digital Collection: Montreal, QC, Canada, 2011; pp. 59–72.
14. Fang, R.; Zhao, S.; Sun, Z.; Wang, D.-W.; Cheng, H.-M.; Li, F. More Reliable Lithium-Sulfur Batteries: Status, Solutions and Prospects. *Adv. Mater.* **2017**, *29*, 1606823. [[CrossRef](#)]
15. Bruce, P.G.; Freunberger, S.A.; Hardwick, L.J.; Tarascon, J.-M. Li-O<sub>2</sub> and Li-S batteries with high energy storage. *Nat. Mater.* **2012**, *11*, 19–29. [[CrossRef](#)] [[PubMed](#)]
16. Fotouhi, A.; Auger, D.J.; O'Neill, L.; Cleaver, T.; Walus, S. Lithium-Sulfur Battery Technology Readiness and Applications—A Review. *Energies* **2017**, *10*, 1937. [[CrossRef](#)]
17. Peng, H.-J.; Huang, J.-Q.; Cheng, X.-B.; Zhang, Q. Review on High-Loading and High-Energy Lithium–Sulfur Batteries. *Adv. Energy Mater.* **2017**, *7*, 1700260. [[CrossRef](#)]
18. Li, C.; Zhang, H.; Otaegui, L.; Singh, G.; Armand, M.; Rodriguez-Martinez, L.M. Estimation of energy density of Li-S batteries with liquid and solid electrolytes. *J. Power Sources* **2016**, *326*, 1–5. [[CrossRef](#)]
19. Durmus, Y.E.; Zhang, H.; Baakes, F.; Desmaizieres, G.; Hayun, H.; Yang, L.; Kolek, M.; Küpers, V.; Janek, J.; Mandler, D.; et al. Side by Side Battery Technologies with Lithium-Ion Based Batteries. *Adv. Energy Mater.* **2020**, *10*, 2000089. [[CrossRef](#)]
20. Huang, X.; Xue, J.; Xiao, M.; Wang, S.; Li, Y.; Zhang, S.; Meng, Y. Comprehensive evaluation of safety performance and failure mechanism analysis for lithium sulfur pouch cells. *Energy Storage Mater.* **2020**, *30*, 87–97. [[CrossRef](#)]
21. Manthiram, A.; Fu, Y.; Chung, S.-H.; Zu, C.; Su, Y.-S. Rechargeable Lithium–Sulfur Batteries. *Chem. Rev.* **2014**, *114*, 11751–11787. [[CrossRef](#)]
22. Yang, C.; Li, P.; Yu, J.; Zhao, L.-D.; Kong, L. Approaching energy-dense and cost-effective lithium–sulfur batteries: From materials chemistry and price considerations. *Energy* **2020**, *201*, 117718. [[CrossRef](#)]
23. Rappold, T.A.; Lackner, K.S. Large scale disposal of waste sulfur: From sulfide fuels to sulfate sequestration. *Energy* **2010**, *35*, 1368–1380. [[CrossRef](#)]
24. Hagen, M.; Hanselmann, D.; Ahlbrecht, K.; Maça, R.; Gerber, D.; Tübke, J. Lithium–Sulfur Cells: The Gap between the State-of-the-Art and the Requirements for High Energy Battery Cells. *Adv. Energy Mater.* **2015**, *5*, 1401986. [[CrossRef](#)]
25. Song, M.-K.; Cairns, E.J.; Zhang, Y. Lithium/sulfur batteries with high specific energy: Old challenges and new opportunities. *Nanoscale* **2013**, *5*, 2186. [[CrossRef](#)] [[PubMed](#)]
26. Moon, S.; Jung, Y.H.; Jung, W.K.; Jung, D.S.; Choi, J.W.; Kim, D.K. Encapsulated Monoclinic Sulfur for Stable Cycling of Li–S Rechargeable Batteries. *Adv. Mater.* **2013**, *25*, 6547–6553. [[CrossRef](#)]
27. Fang, R.; Zhao, S.; Pei, S.; Qian, X.; Hou, P.-X.; Cheng, H.-M.; Liu, C.; Li, F. Toward More Reliable Lithium–Sulfur Batteries: An All-Graphene Cathode Structure. *ACS Nano* **2016**, *10*, 8676–8682. [[CrossRef](#)] [[PubMed](#)]
28. Yin, Y.-X.; Xin, S.; Guo, Y.-G.; Wan, L.-J. Lithium–Sulfur Batteries: Electrochemistry, Materials, and Prospects. *Angew. Chem. Int. Ed.* **2013**, *52*, 13186–13200. [[CrossRef](#)]
29. Ji, X.; Lee, K.T.; Nazar, L.F. A highly ordered nanostructured carbon–sulphur cathode for lithium–sulphur batteries. *Nat. Mater.* **2009**, *8*, 500–506. [[CrossRef](#)] [[PubMed](#)]

30. Yuan, Z.; Peng, H.-J.; Hou, T.-Z.; Huang, J.-Q.; Chen, C.-M.; Wang, D.-W.; Cheng, X.-B.; Wei, F.; Zhang, Q. Powering Lithium–Sulfur Battery Performance by Propelling Polysulfide Redox at Sulfophilic Hosts. *Nano Lett.* **2016**, *16*, 519–527. [CrossRef]
31. Zhao, M.-Q.; Zhang, Q.; Huang, J.-Q.; Tian, G.-L.; Nie, J.-Q.; Peng, H.-J.; Wei, F. Unstacked double-layer templated graphene for high-rate lithium–sulphur batteries. *Nat. Commun.* **2014**, *5*, 1–8. [CrossRef]
32. Li, Z.; Zhang, J.T.; Chen, Y.M.; Li, J.; Lou, X.W. (David) Pie-like electrode design for high-energy density lithium–sulfur batteries. *Nat. Commun.* **2015**, *6*, 8850. [CrossRef]
33. Zhong, Y.; Xia, X.; Deng, S.; Zhan, J.; Fang, R.; Xia, Y.; Wang, X.; Zhang, Q.; Tu, J. Popcorn Inspired Porous Macrocellular Carbon: Rapid Puffing Fabrication from Rice and Its Applications in Lithium–Sulfur Batteries. *Adv. Energy Mater.* **2018**, *8*, 1701110. [CrossRef]
34. Zhou, G.; Paek, E.; Hwang, G.S.; Manthiram, A. Long-life Li/polysulphide batteries with high sulphur loading enabled by lightweight three-dimensional nitrogen/sulphur-codoped graphene sponge. *Nat. Commun.* **2015**, *6*, 7760. [CrossRef]
35. Wei Seh, Z.; Li, W.; Cha, J.J.; Zheng, G.; Yang, Y.; McDowell, M.T.; Hsu, P.-C.; Cui, Y. Sulphur–TiO<sub>2</sub> yolk–shell nanoarchitecture with internal void space for long-cycle lithium–sulphur batteries. *Nat. Commun.* **2013**, *4*, 1331. [CrossRef]
36. Gu, P.-Y.; Zhao, Y.; Xie, J.; Binte Ali, N.; Nie, L.; Xu, Z.J.; Zhang, Q. Improving the Performance of Lithium–Sulfur Batteries by Employing Polyimide Particles as Hosting Matrixes. *ACS Appl. Mater. Interfaces* **2016**, *8*, 7464–7470. [CrossRef]
37. Zeng, F.; Wang, W.; Wang, A.; Yuan, K.; Jin, Z.; Yang, Y. Multidimensional Polycation  $\beta$ -Cyclodextrin Polymer as an Effective Aqueous Binder for High Sulfur Loading Cathode in Lithium–Sulfur Batteries. *ACS Appl. Mater. Interfaces* **2015**, *7*, 26257–26265. [CrossRef]
38. Bao, W.; Zhang, Z.; Gan, Y.; Wang, X.; Lia, J. Enhanced cyclability of sulfur cathodes in lithium-sulfur batteries with Na-alginate as a binder. *J. Energy Chem.* **2013**, *22*, 790–794. [CrossRef]
39. Wang, H.; Ling, M.; Bai, Y.; Chen, S.; Yuan, Y.; Liu, G.; Wu, C.; Wu, F. Cationic polymer binder inhibit shuttle effects through electrostatic confinement in lithium sulfur batteries. *J. Mater. Chem. A* **2018**, *6*, 6959–6966. [CrossRef]
40. Li, G.; Cai, W.; Liu, B.; Li, Z. A multi functional binder with lithium ion conductive polymer and polysulfide absorbents to improve cycleability of lithium–sulfur batteries. *J. Power Sources* **2015**, *294*, 187–192. [CrossRef]
41. Qie, L.; Zu, C.; Manthiram, A. A High Energy Lithium-Sulfur Battery with Ultrahigh-Loading Lithium Polysulfide Cathode and its Failure Mechanism. *Adv. Energy Mater.* **2016**, *6*, 1502459. [CrossRef]
42. Zhang, S.S.; Tran, D.T. Pyrite FeS<sub>2</sub> as an efficient adsorbent of lithium polysulphide for improved lithium–sulphur batteries. *J. Mater. Chem. A* **2016**, *4*, 4371–4374. [CrossRef]
43. Moy, D.; Manivannan, A.; Narayanan, S.R. Direct Measurement of Polysulfide Shuttle Current: A Window into Understanding the Performance of Lithium-Sulfur Cells. *J. Electrochem. Soc.* **2014**, *162*, A1. [CrossRef]
44. Mikhaylik, Y.V.; Akridge, J.R. Polysulfide Shuttle Study in the Li/S Battery System. *J. Electrochem. Soc.* **2004**, *151*, A1969. [CrossRef]
45. Cheon, S.-E.; Ko, K.-S.; Cho, J.-H.; Kim, S.-W.; Chin, E.-Y.; Kim, H.-T. Rechargeable Lithium Sulfur Battery: I. Structural Change of Sulfur Cathode During Discharge and Charge. *J. Electrochem. Soc.* **2003**, *150*, A796. [CrossRef]
46. Hofmann, A.F.; Fronczek, D.N.; Bessler, W.G. Mechanistic modeling of polysulfide shuttle and capacity loss in lithium–sulfur batteries. *J. Power Sources* **2014**, *259*, 300–310. [CrossRef]
47. Fuller, T.F.; Harb, J.N. *Electrochemical Engineering*, 1st ed.; John Wiley & Sons, Incorporated: Hoboken, NJ, USA, 2018; Volume 1, ISBN 978-1-119-44658-3.
48. Ryu, H.S.; Ahn, H.J.; Kim, K.W.; Ahn, J.H.; Cho, K.K.; Nam, T.H. Self-discharge characteristics of lithium/sulfur batteries using TEGDME liquid electrolyte. *Electrochim. Acta* **2006**, *52*, 1563–1566. [CrossRef]
49. Li, S.-Y.; Wang, W.-P.; Duan, H.; Guo, Y.-G. Recent progress on confinement of polysulfides through physical and chemical methods. *J. Energy Chem.* **2018**, *27*, 1555–1565. [CrossRef]
50. Huang, J.-Q.; Zhuang, T.-Z.; Zhang, Q.; Peng, H.-J.; Chen, C.-M.; Wei, F. Permselective Graphene Oxide Membrane for Highly Stable and Anti-Self-Discharge Lithium–Sulfur Batteries. *ACS Nano* **2015**, *9*, 3002–3011. [CrossRef] [PubMed]
51. Li, C.; Ward, A.L.; Doris, S.E.; Pascal, T.A.; Prendergast, D.; Helms, B.A. Polysulfide-Blocking Microporous Polymer Membrane Tailored for Hybrid Li-Sulfur Flow Batteries. *Nano Lett.* **2015**, *15*, 5724–5729. [CrossRef]
52. Liang, X.; Hart, C.; Pang, Q.; Garsuch, A.; Weiss, T.; Nazar, L.F. A highly efficient polysulfide mediator for lithium–sulfur batteries. *Nat. Commun.* **2015**, *6*, 1–8. [CrossRef]
53. Hwa, Y.; Cairns, E.J. Nanostructured Sulfur and Sulfides for Advanced Lithium/Sulfur Cells. *ChemElectroChem* **2020**, *7*, 3927–3942. [CrossRef]
54. Zhao, H.; Deng, N.; Yan, J.; Kang, W.; Ju, J.; Ruan, Y.; Wang, X.; Zhuang, X.; Li, Q.; Cheng, B. A review on anode for lithium-sulfur batteries: Progress and prospects. *Chem. Eng. J.* **2018**, *347*, 343–365. [CrossRef]
55. Ma, L.; Hendrickson, K.E.; Wei, S.; Archer, L.A. Nanomaterials: Science and applications in the lithium–sulfur battery. *Nano Today* **2015**, *10*, 315–338. [CrossRef]
56. He, J.; Manthiram, A. A review on the status and challenges of electrocatalysts in lithium-sulfur batteries. *Energy Storage Mater.* **2019**, *20*, 55–70. [CrossRef]
57. Fan, X.; Sun, W.; Meng, F.; Xing, A.; Liu, J. Advanced chemical strategies for lithium–sulfur batteries: A review. *Green Energy Environ.* **2018**, *3*, 2–19. [CrossRef]

58. Kim, S.; Kim, K.; Park, J.; Sung, Y. Role and Potential of Metal Sulfide Catalysts in Lithium-Sulfur Battery Applications. *ChemCatChem* **2019**, *11*, 2373–2387. [[CrossRef](#)]
59. Burke, K. Perspective on density functional theory. *J. Chem. Phys.* **2012**, *136*, 150901. [[CrossRef](#)]
60. Grotendorst, J. *Modern Methods and Algorithms of Quantum Chemistry: Winterschool, 21–25 February 2000, Forschungszentrum Jülich, Germany. Proceedings*; Grotendorst, J., Ed.; NIC Series; NIC-Directors: Jülich, Germany, 2000; Volume 1, ISBN 978-3-00-005618-5.
61. Liu, Z.; Bertolini, S.; Balbuena, P.B.; Mukherjee, P.P. Li<sub>2</sub>S Film Formation on Lithium Anode Surface of Li–S batteries. *ACS Appl. Mater. Interfaces* **2016**, *8*, 4700–4708. [[CrossRef](#)]
62. Du, G.-Y.; Liu, C.-Y.; Li, E.Y. A DFT Investigation on the Origins of Solvent-Dependent Polysulfide Reduction Mechanism in Rechargeable Li-S Batteries. *Catalysts* **2020**, *10*, 911. [[CrossRef](#)]
63. Arneson, C.; Wawrzyniakowski, Z.D.; Postlewaite, J.T.; Ma, Y. Lithiation and Delithiation Processes in Lithium–Sulfur Batteries from Ab Initio Molecular Dynamics Simulations. *J. Phys. Chem. C* **2018**, *122*, 8769–8779. [[CrossRef](#)]
64. Kamphaus, E.P.; Balbuena, P.B. First-Principles Investigation of Lithium Polysulfide Structure and Behavior in Solution. *J. Phys. Chem. C* **2017**, *121*, 21105–21117. [[CrossRef](#)]
65. Hou, T.-Z.; Chen, X.; Peng, H.-J.; Huang, J.-Q.; Li, B.-Q.; Zhang, Q.; Li, B. Design Principles for Heteroatom-Doped Nanocarbon to Achieve Strong Anchoring of Polysulfides for Lithium–Sulfur Batteries. *Small* **2016**, *12*, 3283–3291. [[CrossRef](#)] [[PubMed](#)]
66. Kamphaus, E.P.; Balbuena, P.B. Long-Chain Polysulfide Retention at the Cathode of Li–S Batteries. *J. Phys. Chem. C* **2016**, *120*, 4296–4305. [[CrossRef](#)]
67. Liang, P.; Zhang, L.; Wang, D.; Man, X.; Shu, H.; Wang, L.; Wan, H.; Du, X.; Wang, H. First-principles explorations of Li<sub>2</sub>S@V2CT hybrid structure as cathode material for lithium-sulfur battery. *Appl. Surf. Sci.* **2019**, *489*, 677–683. [[CrossRef](#)]
68. Sun, Z.; Zhang, J.; Yin, L.; Hu, G.; Fang, R.; Cheng, H.-M.; Li, F. Conductive porous vanadium nitride/graphene composite as chemical anchor of polysulfides for lithium-sulfur batteries. *Nat. Commun.* **2017**, *8*, 14627. [[CrossRef](#)] [[PubMed](#)]
69. Wang, Y.; Zhang, R.; Pang, Y.; Chen, X.; Lang, J.; Xu, J.; Xiao, C.; Li, H.; Xi, K.; Ding, S. Carbon@titanium nitride dual shell nanospheres as multi-functional hosts for lithium sulfur batteries. *Energy Storage Mater.* **2019**, *16*, 228–235. [[CrossRef](#)]
70. Shao, Y.; Wang, Q.; Hu, L.; Pan, H.; Shi, X. BC2N monolayers as promising anchoring materials for lithium-sulfur batteries: First-principles insights. *Carbon* **2019**, *149*, 530–537. [[CrossRef](#)]
71. Park, H.; Siegel, D.J. Tuning the Adsorption of Polysulfides in Lithium–Sulfur Batteries with Metal–Organic Frameworks. *Chem. Mater.* **2017**, *29*, 4932–4939. [[CrossRef](#)]
72. Zhang, Q.; Wang, Y.; Seh, Z.W.; Fu, Z.; Zhang, R.; Cui, Y. Understanding the Anchoring Effect of Two-Dimensional Layered Materials for Lithium–Sulfur Batteries. *Nano Lett.* **2015**, *15*, 3780–3786. [[CrossRef](#)]
73. Wang, Y.; Zhang, R.; Chen, J.; Wu, H.; Lu, S.; Wang, K.; Li, H.; Harris, C.J.; Xi, K.; Kumar, R.V.; et al. Enhancing Catalytic Activity of Titanium Oxide in Lithium–Sulfur Batteries by Band Engineering. *Adv. Energy Mater.* **2019**, *9*, 1900953. [[CrossRef](#)]
74. Tao, X.; Wang, J.; Liu, C.; Wang, H.; Yao, H.; Zheng, G.; Seh, Z.W.; Cai, Q.; Li, W.; Zhou, G.; et al. Balancing surface adsorption and diffusion of lithium-polysulfides on nonconductive oxides for lithium–sulfur battery design. *Nat. Commun.* **2016**, *7*, 11203. [[CrossRef](#)]
75. Yang, X.; Gao, X.; Sun, Q.; Jand, S.P.; Yu, Y.; Zhao, Y.; Li, X.; Adair, K.; Kuo, L.-Y.; Rohrer, J.; et al. Promoting the Transformation of Li<sub>2</sub>S<sub>2</sub> to Li<sub>2</sub>S: Significantly Increasing Utilization of Active Materials for High-Sulfur-Loading Li–S Batteries. *Adv. Mater.* **2019**, *31*, 1901220. [[CrossRef](#)] [[PubMed](#)]
76. Zhang, Q.; Zhang, X.; Li, M.; Liu, J.; Wu, Y. Sulfur-deficient MoS<sub>2-x</sub> promoted lithium polysulfides conversion in lithium-sulfur battery: A first-principles study. *Appl. Surf. Sci.* **2019**, *487*, 452–463. [[CrossRef](#)]
77. Zhou, G.; Zhao, S.; Wang, T.; Yang, S.-Z.; Johannessen, B.; Chen, H.; Liu, C.; Ye, Y.; Wu, Y.; Peng, Y.; et al. Theoretical Calculation Guided Design of Single-Atom Catalysts toward Fast Kinetic and Long-Life Li–S Batteries. *Nano Lett.* **2020**, *20*, 1252–1261. [[CrossRef](#)] [[PubMed](#)]
78. Wang, M.; Fan, L.; Wu, X.; Qiu, Y.; Guan, B.; Wang, Y.; Zhang, N.; Sun, K. Metallic NiSe<sub>2</sub> nanoarrays towards ultralong life and fast Li<sub>2</sub>S oxidation kinetics of Li–S batteries. *J. Mater. Chem. A* **2019**, *7*, 15302–15308. [[CrossRef](#)]
79. Wild, M.; O'Neill, L.; Zhang, T.; Purkayastha, R.; Minton, G.; Marinescu, M.; Offer, G.J. Lithium sulfur batteries, a mechanistic review. *Energy Environ. Sci.* **2015**, *8*, 3477–3494. [[CrossRef](#)]
80. Barchasz, C.; Molton, F.; Duboc, C.; Leprêtre, J.-C.; Patoux, S.; Alloin, F. Lithium/Sulfur Cell Discharge Mechanism: An Original Approach for Intermediate Species Identification. *Anal. Chem.* **2012**, *84*, 3973–3980. [[CrossRef](#)]
81. Wang, Z.; Ye, S.; Wang, H.; He, J.; Huang, Q.; Chang, S. Machine learning method for tight-binding Hamiltonian parameterization from ab-initio band structure. *NPJ Comput. Mater.* **2021**, *7*, 1–10. [[CrossRef](#)]
82. McDonagh, J.L.; Shkurti, A.; Bray, D.J.; Anderson, R.L.; Pyzer-Knapp, E.O. Utilizing Machine Learning for Efficient Parameterization of Coarse Grained Molecular Force Fields. *J. Chem. Inf. Model.* **2019**, *59*, 4278–4288. [[CrossRef](#)]
83. Murillo, M.S.; Marciante, M.; Stanton, L.G. Machine Learning Discovery of Computational Model Efficacy Boundaries. *Phys. Rev. Lett.* **2020**, *125*, 085503. [[CrossRef](#)] [[PubMed](#)]
84. Schmidt, J.; Benavides-Riveros, C.L.; Marques, M.A.L. Machine Learning the Physical Nonlocal Exchange–Correlation Functional of Density-Functional Theory. *J. Phys. Chem. Lett.* **2019**, *10*, 6425–6431. [[CrossRef](#)]
85. Rapaport, D.C. *The Art of Molecular Dynamics Simulation*; Cambridge University Press: Cambridge, UK, 2004; ISBN 978-1-139-45176-5.
86. Park, C.; Kanduč, M.; Chudoba, R.; Ronneburg, A.; Risse, S.; Ballauff, M.; Dzubiella, J. Molecular simulations of electrolyte structure and dynamics in lithium–sulfur battery solvents. *J. Power Sources* **2018**, *373*, 70–78. [[CrossRef](#)]

87. Han, S. Structure and dynamics in the lithium solvation shell of nonaqueous electrolytes. *Sci. Rep.* **2019**, *9*, 5555. [[CrossRef](#)] [[PubMed](#)]
88. Han, K.S.; Chen, J.; Cao, R.; Rajput, N.N.; Murugesan, V.; Shi, L.; Pan, H.; Zhang, J.-G.; Liu, J.; Persson, K.A.; et al. Effects of Anion Mobility on Electrochemical Behaviors of Lithium–Sulfur Batteries. *Chem. Mater.* **2017**, *29*, 9023–9029. [[CrossRef](#)]
89. Babar, S.; Lekakou, C. Molecular modeling of electrolyte and polysulfide ions for lithium-sulfur batteries. *Ionics* **2021**, *27*, 635–642. [[CrossRef](#)]
90. Li, Y.; Romero, N.A.; Lau, K.C. Structure–Property of Lithium–Sulfur Nanoparticles via Molecular Dynamics Simulation. *ACS Appl. Mater. Interfaces* **2018**, *10*, 37575–37585. [[CrossRef](#)]
91. Scheers, J.; Fantini, S.; Johansson, P. A review of electrolytes for lithium–sulphur batteries. *J. Power Sources* **2014**, *255*, 204–218. [[CrossRef](#)]
92. Glueckauf, E. The influence of ionic hydration on activity coefficients in concentrated electrolyte solutions. *Trans. Faraday Soc.* **1955**, *51*, 1235–1244. [[CrossRef](#)]
93. Zhang, L.; Qian, T.; Zhu, X.; Hu, Z.; Wang, M.; Zhang, L.; Jiang, T.; Tian, J.-H.; Yan, C. In situ optical spectroscopy characterization for optimal design of lithium–sulfur batteries. *Chem. Soc. Rev.* **2019**, *48*, 5432–5453. [[CrossRef](#)] [[PubMed](#)]
94. Lyu, Y.; Brusseau, M.L.; Ouni, A.E.; Araujo, J.B.; Su, X. The Gas-Absorption/Chemical-Reaction Method for Measuring Air-Water Interfacial Area in Natural Porous Media. *Water Resour. Res.* **2017**, *53*, 9519–9527. [[CrossRef](#)]
95. Komini Babu, S.; Mohamed, A.I.; Whitacre, J.F.; Litster, S. Multiple imaging mode X-ray computed tomography for distinguishing active and inactive phases in lithium-ion battery cathodes. *J. Power Sources* **2015**, *283*, 314–319. [[CrossRef](#)]
96. He, X.; Ren, J.; Wang, L.; Pu, W.; Jiang, C.; Wan, C. Expansion and shrinkage of the sulfur composite electrode in rechargeable lithium batteries. *J. Power Sources* **2009**, *190*, 154–156. [[CrossRef](#)]
97. Wu, H.-L.; Huff, L.A.; Gewirth, A.A. In Situ Raman Spectroscopy of Sulfur Speciation in Lithium–Sulfur Batteries. *ACS Appl. Mater. Interfaces* **2015**, *7*, 1709–1719. [[CrossRef](#)]
98. Tian, J.-H.; Jiang, T.; Wang, M.; Hu, Z.; Zhu, X.; Zhang, L.; Qian, T.; Yan, C. In Situ/Operando Spectroscopic Characterizations Guide the Compositional and Structural Design of Lithium–Sulfur Batteries. *Small Methods* **2020**, *4*, 1900467. [[CrossRef](#)]
99. Yan, Y.; Cheng, C.; Zhang, L.; Li, Y.; Lu, J. Deciphering the Reaction Mechanism of Lithium–Sulfur Batteries by In Situ/Operando Synchrotron-Based Characterization Techniques. *Adv. Energy Mater.* **2019**, *9*, 1900148. [[CrossRef](#)]
100. Pattnaik, P.; Raghunathan, S.; Kalluri, T.; Bhimalapuram, P.; Jawahar, C.V.; Priyakumar, U.D. Machine Learning for Accurate Force Calculations in Molecular Dynamics Simulations. *J. Phys. Chem. A* **2020**, *124*, 6954–6967. [[CrossRef](#)] [[PubMed](#)]
101. Wang, Y.; Lamim Ribeiro, J.M.; Tiwary, P. Machine learning approaches for analyzing and enhancing molecular dynamics simulations. *Curr. Opin. Struct. Biol.* **2020**, *61*, 139–145. [[CrossRef](#)] [[PubMed](#)]
102. Lu, X.; Bertei, A.; Finegan, D.P.; Tan, C.; Daemi, S.R.; Weaving, J.S.; O'Regan, K.B.; Heenan, T.M.M.; Hinds, G.; Kendrick, E.; et al. 3D microstructure design of lithium-ion battery electrodes assisted by X-ray nano-computed tomography and modelling. *Nat. Commun.* **2020**, *11*, 2079. [[CrossRef](#)] [[PubMed](#)]
103. Chen, S.; Doolen, G.D. Lattice boltzmann method for fluid flows. *Annu. Rev. Fluid Mech.* **1998**, *30*, 329–364. [[CrossRef](#)]
104. Cao, H.; Jia, X.; Li, Y.; Amador, C.; Ding, Y. CFD-DNS simulation of irregular-shaped particle dissolution. *Particuology* **2020**, *50*, 144–155. [[CrossRef](#)]
105. Kumaresan, K.; Mikhaylik, Y.; White, R.E. A Mathematical Model for a Lithium–Sulfur Cell. *J. Electrochem. Soc.* **2008**, *155*, A576. [[CrossRef](#)]
106. Zhang, T.; Marinescu, M.; O'Neill, L.; Wild, M.; Offer, G. Modeling the voltage loss mechanisms in lithium–sulfur cells: The importance of electrolyte resistance and precipitation kinetics. *Phys. Chem. Chem. Phys.* **2015**, *17*, 22581–22586. [[CrossRef](#)]
107. Marinescu, M.; Zhang, T.; Offer, G.J. A zero dimensional model of lithium–sulfur batteries during charge and discharge. *Phys. Chem. Chem. Phys.* **2016**, *18*, 584–593. [[CrossRef](#)]
108. Marinescu, M.; O'Neill, L.; Zhang, T.; Walus, S.; Wilson, T.E.; Offer, G.J. Irreversible vs Reversible Capacity Fade of Lithium-Sulfur Batteries during Cycling: The Effects of Precipitation and Shuttle. *J. Electrochem. Soc.* **2017**, *165*, A6107. [[CrossRef](#)]
109. Hua, X.; Zhang, T.; Offer, G.J.; Marinescu, M. Towards online tracking of the shuttle effect in lithium sulfur batteries using differential thermal voltammetry. *J. Energy Storage* **2019**, *21*, 765–772. [[CrossRef](#)]
110. Ghaznavi, M.; Chen, P. Analysis of a Mathematical Model of Lithium-Sulfur Cells Part III: Electrochemical Reaction Kinetics, Transport Properties and Charging. *Electrochim. Acta* **2014**, *137*, 575–585. [[CrossRef](#)]
111. Danner, T.; Zhu, G.; Hofmann, A.F.; Latz, A. Modeling of nano-structured cathodes for improved lithium-sulfur batteries. *Electrochim. Acta* **2015**, *184*, 124–133. [[CrossRef](#)]
112. Thangavel, V.; Xue, K.-H.; Mammeri, Y.; Quiroga, M.; Mastouri, A.; Guéry, C.; Johansson, P.; Morcrette, M.; Franco, A.A. A Microstructurally Resolved Model for Li-S Batteries Assessing the Impact of the Cathode Design on the Discharge Performance. *J. Electrochem. Soc.* **2016**, *163*, A2817. [[CrossRef](#)]
113. Ren, Y.X.; Zhao, T.S.; Liu, M.; Tan, P.; Zeng, Y.K. Modeling of lithium-sulfur batteries incorporating the effect of  $\text{Li}_2\text{S}$  precipitation. *J. Power Sources* **2016**, *336*, 115–125. [[CrossRef](#)]
114. Wen, G.; Rehman, S.; Tranter, T.G.; Ghosh, D.; Chen, Z.; Gostick, J.T.; Pope, M.A. Insights into Multiphase Reactions during Self-Discharge of Li-S Batteries. *Chem. Mater.* **2020**, *32*, 4518–4526. [[CrossRef](#)]
115. Price, C.W. Use of Kolmogorov-Johnson-Mehl-Avrami kinetics in recrystallization of metals and crystallization of metallic glasses. *Acta Metall. Mater.* **1990**, *38*, 727–738. [[CrossRef](#)]

116. Andrei, P.; Shen, C.; Zheng, J.P. Theoretical and experimental analysis of precipitation and solubility effects in lithium-sulfur batteries. *Electrochim. Acta* **2018**, *284*, 469–484. [[CrossRef](#)]
117. Yoreo, J.J.D.; Vekilov, P.G. Principles of Crystal Nucleation and Growth. *Rev. Mineral. Geochem.* **2003**, *54*, 57–93. [[CrossRef](#)]
118. Danner, T.; Latz, A. On the influence of nucleation and growth of S<sub>8</sub> and Li<sub>2</sub>S in lithium-sulfur batteries. *Electrochim. Acta* **2019**, *322*, 134719. [[CrossRef](#)]
119. Xiong, C.; Zhao, T.S.; Ren, Y.X.; Jiang, H.R.; Zhou, X.L. Mathematical modeling of the charging process of Li-S batteries by incorporating the size-dependent Li<sub>2</sub>S dissolution. *Electrochim. Acta* **2019**, *296*, 954–963. [[CrossRef](#)]
120. Tan, C.; Kok, M.D.R.; Daemi, S.R.; Brett, D.J.L.; Shearing, P.R. Three-dimensional image based modelling of transport parameters in lithium-sulfur batteries. *Phys. Chem. Chem. Phys.* **2019**, *21*, 4145–4154. [[CrossRef](#)]
121. Tan, C.; Heenan, T.M.M.; Ziesche, R.F.; Daemi, S.R.; Hack, J.; Maier, M.; Marathe, S.; Rau, C.; Brett, D.J.L.; Shearing, P.R. Four-Dimensional Studies of Morphology Evolution in Lithium-Sulfur Batteries. *ACS Appl. Energy Mater.* **2018**, *1*, 5090–5100. [[CrossRef](#)]
122. Thangavel, V.; Guerrero, O.X.; Quiroga, M.; Mikala, A.M.; Rucci, A.; Franco, A.A. A three dimensional kinetic Monte Carlo model for simulating the carbon/sulfur mesostructural evolutions of discharging lithium sulfur batteries. *Energy Storage Mater.* **2020**, *24*, 472–485. [[CrossRef](#)]
123. Mistry, A.; Mukherjee, P.P. Precipitation–Microstructure Interactions in the Li-Sulfur Battery Electrode. *J. Phys. Chem. C* **2017**, *121*, 26256–26264. [[CrossRef](#)]
124. Agnaou, M.; Sadeghi, M.A.; Tranter, T.G.; Gostick, J.T. Modeling transport of charged species in pore networks: Solution of the Nernst–Planck equations coupled with fluid flow and charge conservation equations. *Comput. Geosci.* **2020**, *140*, 104505. [[CrossRef](#)]
125. DuBeshter, T.; Sinha, P.K.; Sakars, A.; Fly, G.W.; Jorne, J. Measurement of Tortuosity and Porosity of Porous Battery Electrodes. *J. Electrochem. Soc.* **2014**, *161*, A599–A605. [[CrossRef](#)]
126. Liu, B.; Fang, R.; Xie, D.; Zhang, W.; Huang, H.; Xia, Y.; Wang, X.; Xia, X.; Tu, J. Revisiting Scientific Issues for Industrial Applications of Lithium–Sulfur Batteries. *Energy Environ. Mater.* **2018**, *1*, 196–208. [[CrossRef](#)]
127. Miller, E.C.; Toney, M.F. X-Ray Studies of Energy Materials. In *Synchrotron Light Sources and Free-Electron Lasers: Accelerator Physics, Instrumentation and Science Applications*; Jaeschke, E.J., Khan, S., Schneider, J.R., Hastings, J.B., Eds.; Springer International Publishing: Cham, Switzerland, 2020; pp. 1803–1824, ISBN 978-3-030-23201-6.
128. Safari, M.; Kwok, C.Y.; Nazar, L.F. Transport Properties of Polysulfide Species in Lithium–Sulfur Battery Electrolytes: Coupling of Experiment and Theory. *ACS Cent. Sci.* **2016**, *2*, 560–568. [[CrossRef](#)] [[PubMed](#)]
129. Shah, K.; Subramaniam, A.; Mishra, L.; Jang, T.; Bazant, M.Z.; Braatz, R.D.; Subramanian, V.R. Editors’ Choice—Perspective—Challenges in Moving to Multiscale Battery Models: Where Electrochemistry Meets and Demands More from Math. *J. Electrochem. Soc.* **2020**, *167*, 133501. [[CrossRef](#)]
130. Franco, A.A.; Rucci, A.; Brandell, D.; Frayret, C.; Gaberscek, M.; Jankowski, P.; Johansson, P. Boosting Rechargeable Batteries R&D by Multiscale Modeling: Myth or Reality? *Chem. Rev.* **2019**, *119*, 4569–4627.
131. Mistry, A.; Franco, A.A.; Cooper, S.J.; Roberts, S.A.; Viswanathan, V. How Machine Learning Will Revolutionize Electrochemical Sciences. *ACS Energy Lett.* **2021**, *6*, 1422–1431. [[CrossRef](#)] [[PubMed](#)]
132. Kolodziejczyk, F.; Mortazavi, B.; Rabczuk, T.; Zhuang, X. Machine learning assisted multiscale modeling of composite phase change materials for Li-ion batteries’ thermal management. *Int. J. Heat Mass Transf.* **2021**, *172*, 121199. [[CrossRef](#)]
133. Kilic, A.; Odabaşı, Ç.; Yıldırım, R.; Eroglu, D. Assessment of critical materials and cell design factors for high performance lithium-sulfur batteries using machine learning. *Chem. Eng. J.* **2020**, *390*, 124117. [[CrossRef](#)]
134. Barrett, D.H.; Haruna, A. Artificial intelligence and machine learning for targeted energy storage solutions. *Curr. Opin. Electrochem.* **2020**, *21*, 160–166. [[CrossRef](#)]
135. Evers, S.; Nazar, L.F. New Approaches for High Energy Density Lithium–Sulfur Battery Cathodes. *Acc. Chem. Res.* **2013**, *46*, 1135–1143. [[CrossRef](#)]
136. Liu, M.; Jiang, H.R.; Ren, Y.X.; Zhou, D.; Kang, F.Y.; Zhao, T.S. In-situ Fabrication of a Freestanding Acrylate-based Hierarchical Electrolyte for Lithium-sulfur Batteries. *Electrochim. Acta* **2016**, *213*, 871–878. [[CrossRef](#)]
137. Feng, L.; Ji, Y.; Zhu, Z.; Yu, P.; Fu, X.; Yang, M.; Wang, Y.; Yang, W. Rational design and superfast production of biomimetic, calendering-compatible, catalytic, sulfur-rich secondary particles for advanced lithium-sulfur batteries. *Energy Storage Mater.* **2021**, *40*, 415–425. [[CrossRef](#)]
138. Thomitzek, M.; Schmidt, O.; Röder, F.; Krewer, U.; Herrmann, C.; Thiede, S. Simulating Process-Product Interdependencies in Battery Production Systems. *Procedia CIRP* **2018**, *72*, 346–351. [[CrossRef](#)]
139. Schmidt, O.; Thomitzek, M.; Röder, F.; Thiede, S.; Herrmann, C.; Krewer, U. Modeling the Impact of Manufacturing Uncertainties on Lithium-Ion Batteries. *J. Electrochem. Soc.* **2020**, *167*, 060501. [[CrossRef](#)]
140. Ngandjong, A.C.; Lombardo, T.; Primo, E.N.; Chouchane, M.; Shodiev, A.; Arcelus, O.; Franco, A.A. Investigating electrode calendering and its impact on electrochemical performance by means of a new discrete element method model: Towards a digital twin of Li-Ion battery manufacturing. *J. Power Sources* **2021**, *485*, 229320. [[CrossRef](#)]
141. Fan, F.Y.; Woodford, W.H.; Li, Z.; Baram, N.; Smith, K.C.; Helal, A.; McKinley, G.H.; Carter, W.C.; Chiang, Y.-M. Polysulfide Flow Batteries Enabled by Percolating Nanoscale Conductor Networks. *Nano Lett.* **2014**, *14*, 2210–2218. [[CrossRef](#)]

142. Liang, J.; Sun, Z.-H.; Li, F.; Cheng, H.-M. Carbon materials for Li–S batteries: Functional evolution and performance improvement. *Energy Storage Mater.* **2016**, *2*, 76–106. [[CrossRef](#)]
143. Eftekhari, A.; Kim, D.-W. Cathode materials for lithium–sulfur batteries: A practical perspective. *J. Mater. Chem. A* **2017**, *5*, 17734–17776. [[CrossRef](#)]
144. Huang, L.; Li, J.; Liu, B.; Li, Y.; Shen, S.; Deng, S.; Lu, C.; Zhang, W.; Xia, Y.; Pan, G.; et al. Electrode Design for Lithium–Sulfur Batteries: Problems and Solutions. *Adv. Funct. Mater.* **2020**, *30*, 1910375. [[CrossRef](#)]
145. Hagen, M.; Fanz, P.; Tübke, J. Cell energy density and electrolyte/sulfur ratio in Li–S cells. *J. Power Sources* **2014**, *264*, 30–34. [[CrossRef](#)]
146. Mikhaylik, Y.V.; Kovalev, I.; Schock, R.; Kumaresan, K.; Xu, J.; Affinito, J. High Energy Rechargeable Li–S Cells for EV Application: Status, Remaining Problems and Solutions. *ECS Trans.* **2010**, *25*, 23. [[CrossRef](#)]
147. Dörfler, S.; Althues, H.; Härtel, P.; Abendroth, T.; Schumm, B.; Kaskel, S. Challenges and Key Parameters of Lithium–Sulfur Batteries on Pouch Cell Level. *Joule* **2020**, *4*, 539–554. [[CrossRef](#)]
148. Bhargav, A.; He, J.; Gupta, A.; Manthiram, A. Lithium–Sulfur Batteries: Attaining the Critical Metrics. *Joule* **2020**, *4*, 285–291. [[CrossRef](#)]
149. Hwa, Y.; Kim, H.W.; Shen, H.; Parkinson, D.Y.; McCloskey, B.D.; Cairns, E.J. A sustainable sulfur–carbonaceous composite electrode toward high specific energy rechargeable cells. *Mater. Horiz.* **2020**, *7*, 524–529. [[CrossRef](#)]
150. Lv, D.; Zheng, J.; Li, Q.; Xie, X.; Ferrara, S.; Nie, Z.; Mehdi, L.B.; Browning, N.D.; Zhang, J.-G.; Graff, G.L.; et al. High Energy Density Lithium–Sulfur Batteries: Challenges of Thick Sulfur Cathodes. *Adv. Energy Mater.* **2015**, *5*, 1402290. [[CrossRef](#)]
151. Chung, S.-H.; Manthiram, A. Designing Lithium–Sulfur Cells with Practically Necessary Parameters. *Joule* **2018**, *2*, 710–724. [[CrossRef](#)]
152. Li, M.; Zhang, Y.; Bai, Z.; Liu, W.W.; Liu, T.; Gim, J.; Jiang, G.; Yuan, Y.; Luo, D.; Feng, K.; et al. A Lithium–Sulfur Battery using a 2D Current Collector Architecture with a Large-Sized Sulfur Host Operated under High Areal Loading and Low E/S Ratio. *Adv. Mater.* **2018**, *30*, 1804271. [[CrossRef](#)]
153. Wang, H.; Liu, Y.; Li, Y.; Cui, Y. Lithium Metal Anode Materials Design: Interphase and Host. *Electrochem. Energy Rev.* **2019**, *2*, 509–517. [[CrossRef](#)]
154. Aurbach, D.; Zinigrad, E.; Cohen, Y.; Teller, H. A short review of failure mechanisms of lithium metal and lithiated graphite anodes in liquid electrolyte solutions. *Solid State Ion.* **2002**, *148*, 405–416. [[CrossRef](#)]
155. Chen, X.; Hou, T.; Persson, K.A.; Zhang, Q. Combining theory and experiment in lithium–sulfur batteries: Current progress and future perspectives. *Mater. Today* **2019**, *22*, 142–158. [[CrossRef](#)]
156. Park, M.S.; Ma, S.B.; Lee, D.J.; Im, D.; Doo, S.-G.; Yamamoto, O. A Highly Reversible Lithium Metal Anode. *Sci. Rep.* **2014**, *4*, 3815. [[CrossRef](#)] [[PubMed](#)]
157. Schmuck, R.; Wagner, R.; Hörpel, G.; Placke, T.; Winter, M. Performance and cost of materials for lithium-based rechargeable automotive batteries. *Nat. Energy* **2018**, *3*, 267–278. [[CrossRef](#)]
158. Ye, Y.; Song, M.-K.; Xu, Y.; Nie, K.; Liu, Y.; Feng, J.; Sun, X.; Cairns, E.J.; Zhang, Y.; Guo, J. Lithium nitrate: A double-edged sword in the rechargeable lithium–sulfur cell. *Energy Storage Mater.* **2019**, *16*, 498–504. [[CrossRef](#)]
159. Qu, C.; Chen, Y.; Yang, X.; Zhang, H.; Li, X.; Zhang, H. LiNO<sub>3</sub>-free electrolyte for Li–S battery: A solvent of choice with low K<sub>sp</sub> of polysulfide and low dendrite of lithium. *Nano Energy* **2017**, *39*, 262–272. [[CrossRef](#)]
160. Suo, L.; Hu, Y.-S.; Li, H.; Armand, M.; Chen, L. A new class of Solvent-in-Salt electrolyte for high-energy rechargeable metallic lithium batteries. *Nat. Commun.* **2013**, *4*, 1481. [[CrossRef](#)]
161. Weber, R.; Genovese, M.; Louli, A.J.; Hames, S.; Martin, C.; Hill, I.G.; Dahn, J.R. Long cycle life and dendrite-free lithium morphology in anode-free lithium pouch cells enabled by a dual-salt liquid electrolyte. *Nat. Energy* **2019**, *4*, 683–689. [[CrossRef](#)]
162. Yue, J.; Yan, M.; Yin, Y.-X.; Guo, Y.-G. Progress of the Interface Design in All-Solid-State Li–S Batteries. *Adv. Funct. Mater.* **2018**, *28*, 1707533. [[CrossRef](#)]
163. Lei, D.; Shi, K.; Ye, H.; Wan, Z.; Wang, Y.; Shen, L.; Li, B.; Yang, Q.-H.; Kang, F.; He, Y.-B. Solid-State Electrolytes: Progress and Perspective of Solid-State Lithium–Sulfur Batteries (Adv. Funct. Mater. 38/2018). *Adv. Funct. Mater.* **2018**, *28*, 1870272. [[CrossRef](#)]
164. Umeshbabu, E.; Zheng, B.; Yang, Y. Recent Progress in All-Solid-State Lithium–Sulfur Batteries Using High Li-Ion Conductive Solid Electrolytes. *Electrochem. Energy Rev.* **2019**, *2*, 199–230. [[CrossRef](#)]
165. Deimede, D.; Elmasides, C. Separators for Lithium-Ion Batteries: A Review on the Production Processes and Recent Developments. *Energy Technol.* **2015**, *3*, 453–468. [[CrossRef](#)]
166. Xiang, Y.; Li, J.; Lei, J.; Liu, D.; Xie, Z.; Qu, D.; Li, K.; Deng, T.; Tang, H. Advanced Separators for Lithium-Ion and Lithium–Sulfur Batteries: A Review of Recent Progress. *ChemSusChem* **2016**, *9*, 1–18. [[CrossRef](#)]
167. Deng, N.; Kang, W.; Liu, Y.; Ju, J.; Wu, D.; Lia, L.; Hassan, B.S.; Cheng, B. A review on separators for lithium–sulfur battery: Progress and prospects. *J. Power Sources* **2016**, *331*, 132–155. [[CrossRef](#)]
168. Wood, D.L.; Li, J.; Daniel, C. Prospects for reducing the processing cost of lithium ion batteries. *J. Power Sources* **2015**, *275*, 234–242. [[CrossRef](#)]